Electronic Supplementary Information (ESI) for "**In Vivo Near-Infrared and Cerenkov Luminescence Imaging of Amyloid-*β* Deposits in the Brain: A Fluorinated Small Molecule Used for Dual-Modality Imaging**"

Hualong Fu,[a] Cheng Peng,[b] Zhigang Liang,[b] Jiapei Dai,[c] Boli Liu[a] and Mengchao Cui,*[a]

[a]Key Laboratory of Radiopharmaceuticals, Ministry of Education, College of Chemistry, Beijing Normal University, Beijing 100875, PR China

[b]Department of Nuclear Medicine, Xuanwu Hospital, Capital Medical University, Beijing 100053, PR China

[c]Wuhan Institute for Neuroscience and Neuroengineering, South-Central University for Nationalities, Wuhan 430074, PR China

Corresponding Author:

*Tel/Fax: +86-10-58808891. E-mail: cmc@bnu.edu.cn (M. Cui)

Table of Contents

General remarks. All chemicals and solvents were commercial products and were used without further purification. ^{1}H NMR (400 MHz) and ^{13}C NMR (100 MHz) spectra were acquired on Bruker Avance III NMR spectrometers in $CDCl_3$ or DMSO-d_6 solutions at room temperature with trimethylsilyl (TMS) as an internal standard and the multiplicity is defined by s (singlet), d (doublet), t (triplet), or m (multiplet). Mass spectra were acquired with the Surveyor MSQ Plus (Supporting Information) (Waltham, MA, USA) instrument. The synthetic trifluoroacetic acid salt forms of peptides A$\beta_{1–42}$ was obtained from Osaka Peptide Institute, Inc. (Osaka, Japan) and aggregated for in vitro studies using the previously reported procedures.[1] All spectroscopic measurements were conducted using a spectrofluorophotometer (RF-5301PC, Shimadzu, Japan) and a UV spectrophotometer (UV-2450, Shimadzu, Japan). Fluorescent microscope observation was performed on the Axio Observer Z1 inverted fluorescence microscope (Zeiss, Germany) that was equipped with DAPI, AF488, and AF546 filter sets. In the measurement of the brain uptake of **4b** and **4c**, HPLC analysis was performed on an Agilent 1260 Infinity Quaternary LC (Agilent Technologies, the USA) system using a Cosmosil packed column (5C18-AR-II, 4.6 × 150 mm) with a binary gradient elution system, while the mobile phases A and B were separately water and acetonitrile at a flow rate of 1.0 mL/min.

Fluorine-18 was kindly provided by Xuanwu Hospital, Capital Medical University. HPLC purification and analysis of radiolabeled ligands were performed on a Shimadzu SCL-20 AVP equipped with a Bioscan Flow Count 3200 NaI/PMT γ-radiation scintillation detector and a SPD-20A UV detector. A Venusil MP C18 reverse phase column (Bonna-Agela Technologies, 5 μm, 10 × 250 mm) was used for separations and purity determinations with a binary gradient system (acetonitrile and water) at a flow rate of 4.0 mL/min. HPLC analysis of metabolic samples was conducted on a Cosmosil packed column (5C18-AR-II, 4.6 × 150 mm) with a binary gradient system (acetonitrile and water) at a flow rate of 1.0 mL/min.

Human brain sections were obtained from the Chinese Brain Bank Center. Normal ICR mice (5 weeks, male) that were used for BBB penetration test and nude mice (BALB/c nude, 6 weeks, female) that were used for in vivo NIR imaging were purchased from the Vital River Laboratory Animal Technology Co. Ltd., Beijing, China. Tg mice (C57BL6, APPswe/PSEN1) and WT mice (C57BL6) that were used for in vitro histology, in vivo NIR imaging, and ex vivo fluorescent staining were purchased from the Institute of Laboratory Animal Science, Chinese Academy of Medical Sciences.

All experiments requiring the use of mice were approved by the animal care committee of Beijing Normal University.

Chemistry.

Compounds **1a-c** were prepared by our previously reported procedures.[2]

2-((6-Formylnaphthalen-2-yl)(methyl)amino)ethyl 4-methylbenzenesulfonate (**2a**) To the solution of 6-((2-hydroxyethyl)(methyl)amino)-2-naphthaldehyde (422.4 mg, 1.8 mmol) in anhydrous CH_2Cl_2 was added 4-toluene sulfonyl chloride (TsCl, 1.5 g, 7.7 mmol) and triethylamine (1.5 mL, 10.8 mmol). The resulting mixture was stirred for 3 h at 40 ℃. After the organic phase was evaporated, the residue was purified by column chromatography using petroleum ether/ethyl acetate (4:1, v:v) to give a yellow solid (561.1 mg, 79.5%). ^{1}H NMR (400 MHz, $CDCl_3$) δ 10.03 (s, 1H), 8.15 (s, 1H), 7.84 (dd, *J* = 8.6, 1.4 Hz, 1H), 7.78 (d, *J* = 9.1 Hz, 1H), 7.66 (d, *J* = 8.3 Hz, 2H), 7.62 (d, *J* = 8.6 Hz, 1H), 7.15 (d, *J* = 8.1 Hz, 2H), 7.04 (dd, *J* = 9.1, 2.5 Hz, 1H), 6.78 (d, *J* = 1.9 Hz, 1H), 4.26 (t, *J* = 5.7 Hz, 2H), 3.79 (t, *J* = 5.8 Hz, 2H), 3.06 (s, 3H), 2.29 (s, 3H). ^{13}C NMR (100.6 MHz, $CDCl_3$) δ: 191.91, 148.63, 145.12, 138.59, 134.69, 132.63, 131.15, 131.05, 129.88, 127.88, 127.08, 125.56, 123.78, 115.94, 106.03, 66.92, 51.30, 39.45, 21.65.

(*E*)-2-(methyl(6-(3-oxoprop-1-en-1-yl)naphthalen-2-yl)amino)ethyl 4-methylbenzenesulfonate (**2b**) The same procedures as described above to prepare compound **2a** was followed to get compound **2b** as a yellow solid (105.0 mg, 59.6%). ^{1}H NMR (400 MHz, $CDCl_3$) δ 9.72 (d, *J* = 7.7 Hz, 1H), 7.83 (s, 1H), 7.70 (d, *J* = 9.1 Hz, 1H), 7.66 (d, *J* = 8.3 Hz, 2H), 7.60 (s, 2H), 7.58 (d, *J* = 16.4 Hz, 1H), 7.17 (d, *J* = 8.1 Hz, 2H), 7.04 (dd, *J* = 9.1, 2.2 Hz, 1H), 6.84 (s, 1H), 6.76 (dd, *J* = 15.8, 7.7 Hz, 1H), 4.27 (t, *J* = 5.7 Hz, 2H), 3.78 (t, *J* = 5.7 Hz, 2H), 3.05 (s, 3H), 2.31 (s, 3H). ^{13}C NMR (100.6 MHz, $CDCl_3$) δ: 193.88, 153.66, 147.78, 145.06, 136.69, 132.72, 130.91, 130.26, 129.87, 128.10, 127.90, 127.19, 126.90, 126.31, 124.42, 115.98, 106.19, 67.00, 51.36, 39.39, 21.66.

2-(Methyl(6-((1*E*,3*E*)-5-oxopenta-1,3-dien-1-yl)naphthalen-2-yl)amino)ethyl 4-methylbenzenesulfonate (**2c**) The same procedure as described above to prepare compound **2a** was followed to get compound **2c** as a yellow solid (45.7 mg, 63.6%). ^{1}H NMR (400 MHz, $CDCl_3$) δ 9.62 (d, *J* = 8.0 Hz, 1H), 7.72 (s, 1H), 7.67 (d, *J* = 8.3 Hz, 2H), 7.64 (d, *J* = 9.3 Hz, 1H), 7.58 (s, 2H), 7.32 (dd, *J* = 15.1, 10.5 Hz, 1H), 7.16 (d, *J* = 7.8 Hz, 2H), 7.10 (d, *J* = 15.2 Hz, 1H), 7.06-7.00 (m, 1H), 6.98 (dd, *J* = 9.1, 2.5 Hz, 1H), 6.74 (d, *J* = 1.9 Hz, 1H), 6.27 (dd, *J* = 15.1, 8.0 Hz, 1H), 4.24 (t, *J* = 5.8 Hz, 2H), 3.76 (t, *J* = 5.8 Hz, 2H), 3.02 (s, 3H), 2.31 (s, 3H). ^{13}C NMR (100.6 MHz, $CDCl_3$) δ:

193.71, 152.91, 147.25, 145.04, 143.39, 135.84, 132.75, 130.66, 129.87, 129.82, 129.75, 129.05, 127.90, 127.05, 126.61, 124.65, 124.17, 115.95, 106.34, 67.09, 51.40, 39.36, 21.65.

6-((2-Fluoroethyl)(methyl)amino)-2-naphthaldehyde (**3a**) To the solution of compound **2a** (256.6 mg, 0.67 mmol) in anhydrous THF (10 mL) was added tetrabutylammonium fluoride (TBAF, 1 M in THF, 2.6 mL, 2.6 mmol). The reaction mixture was stirred for 3 h at 50 ℃, and then the oily liquid was given after the solvent was removed in vacuum. The oily liquid was washed with water (30 mL) and extracted with CH_2Cl_2 (3×25 mL). In the following, the organic phase was dried over anhydrous magnesium sulfate. Solvent was removed in vacuum and the residue was purified by flashing column chromatography (petroleum ether/ethyl acetate = 4:1, v:v) to give compound **3a** as a yellowish solid (86.1 mg, 55.6%). ^{1}H NMR (400 MHz, $CDCl_3$) δ 10.02 (s, 1H), 8.16 (s, 1H), 7.85 (d, *J* = 1.9 Hz, 1H), 7.83 (s, 1H), 7.67 (d, *J* = 8.6 Hz, 1H), 7.18 (dd, *J* = 9.1, 2.6 Hz, 1H), 6.93 (d, *J* = 2.3 Hz, 1H), 4.68 (dt, *J* = 47.1, 5.1 Hz, 2H), 3.82 (dt, *J* = 24.5, 5.1 Hz, 2H), 3.18 (s, 3H). ^{13}C NMR (100.6 MHz, $CDCl_3$) δ: 191.91, 149.43, 138.76, 134.76, 131.09, 131.04, 127.04, 125.48, 123.76, 116.19, 105.87, 81.86 (d, $^1J_{CF}$ = 169.1 Hz), 52.66 (d, $^2J_{CF}$ = 21.1 Hz), 39.33.

(*E*)-3-(6-((2-fluoroethyl)(methyl)amino)naphthalen-2-yl)acrylaldehyde (**3b**) The same procedure as described above to prepare compound **3a** was followed, and a yellow solid compound **3b** (99.7 mg, 37.9%) was obtained by flashing column chromatography using CH_2Cl_2/ethyl acetate = 40:1. ^{1}H NMR (400 MHz, $CDCl_3$) δ 9.72 (d, *J* = 7.8 Hz, 1H), 7.85 (s, 1H), 7.77 (d, *J* = 9.1 Hz, 1H), 7.67 (d, *J* = 8.6 Hz, 1H), 7.61 (d, *J* = 3.0 Hz, 1H), 7.58 (d, *J* = 11.4 Hz, 1H), 7.19 (d, *J* = 7.5 Hz, 1H), 7.02 (s, 1H), 6.76 (dd, *J* = 15.8, 7.8 Hz, 1H), 4.70 (dt, *J* = 47.1, 5.0 Hz, 2H), 3.81 (dt, *J* = 24.7, 5.1 Hz, 2H), 3.18 (s, 3H). ^{13}C NMR (100.6 MHz, $CDCl_3$) δ: 193.87, 153.76, 148.57, 136.84, 130.98, 130.29, 127.99, 127.16, 126.81, 126.27, 124.42, 116.27, 106.11, 81.90 (d, $^1J_{CF}$ = 171.0 Hz), 52.76 (d, $^2J_{CF}$ = 21.1 Hz), 39.33.

(2*E*,4*E*)-5-(6-((2-fluoroethyl)(methyl)amino)naphthalen-2-yl)penta-2,4-dienal (**3c**) The same procedure as described above to prepare compound **3a** was followed, and compound **3c** was obtained by flashing column chromatography using petroleum ether/ethyl acetate = 4:1 (v:v) as an orange solid (35.0 mg, 65.0%). ^{1}H NMR (400 MHz, $CDCl_3$) δ 9.62 (d, *J* = 8.0 Hz, 1H), 7.75 (s, 1H), 7.73 (d, *J* = 11.0 Hz, 1H), 7.64 (d, *J* = 8.7 Hz, 1H), 7.60 (d, *J* = 8.8 Hz, 1H), 7.31 (dd, *J* = 15.1, 10.5 Hz, 1H), 7.17 (d, *J* = 9.7 Hz, 1H), 7.11 (s, 1H), 7.08-7.04 (m, 1H), 7.01 (d, *J* = 4.5 Hz, 1H), 6.27 (dd, *J* = 15.1, 8.0 Hz, 1H), 4.69 (dt, *J* = 47.1, 5.1 Hz, 2H), 3.79 (dt, *J* = 24.5, 5.1 Hz, 2H), 3.16 (s, 3H). ^{13}C NMR

(100.6 MHz, $CDCl_3$) δ: 193.70, 152.94, 148.03, 143.47, 135.98, 130.61, 129.86, 129.65, 129.12, 127.03, 126.57, 124.55, 124.16, 116.26, 106.29, 81.95 (d, $^1J_{CF}$ = 170.0 Hz), 52.85 (d, $^2J_{CF}$ = 20.1 Hz), 39.34.

Fluorinated DANIR (FDANIR) probes **4a**, **4b** and **4c**. Compounds **4a-c** were synthesized by following our previously reported procedures.[2]

2-((6-((2-Fluoroethyl)(methyl)amino)naphthalen-2-yl)methylene)malononitrile (**4a**) A red solid (33.6 mg, 54.7%) was obtained. Mp 138.7−139.9 ℃. ^{1}H NMR (400 MHz, $CDCl_3$) δ 8.09 (s, 1H), 7.97 (dd, *J* = 8.8, 1.8 Hz, 1H), 7.78 (d, *J* = 9.2 Hz, 1H), 7.71 (s, 1H), 7.63 (d, *J* = 8.8 Hz, 1H), 7.17 (dd, *J* = 9.2, 2.5 Hz, 1H), 6.89 (d, *J* = 2.4 Hz, 1H), 4.69 (dt, *J* = 47.0, 5.0 Hz, 2H), 3.84 (dt, *J* = 24.8, 5.0 Hz, 2H), 3.21 (s, 3H). ^{13}C NMR (100.6 MHz, $CDCl_3$) δ: 159.27, 150.16, 138.39, 135.08, 131.51, 127.27, 125.35, 125.28, 124.94, 116.44, 115.05, 113.91, 105.63, 81.64 (d, $^1J_{CF}$ = 170.1 Hz), 77.44, 52.47 (d, $^2J_{CF}$ = 20.9 Hz), 39.27. MS: m/z calcd for $[C_{17}H_{14}FN_3 + H]^+$ 280.1, found 280.0.

(*E*)-2-(3-(6-((2-fluoroethyl)(methyl)amino)naphthalen-2-yl)allylidene)malononitrile (**4b**) A dark red solid (57.4 mg, 62.7%) was obtained. Mp 174.1−175.4 ℃. ^{1}H NMR (400 MHz, $CDCl_3$) δ 7.85 (s, 1H), 7.76 (d, *J* = 9.1 Hz, 1H), 7.66 (d, *J* = 8.7 Hz, 1H), 7.63 (s, 1H), 7.60 (d, *J* = 11.3 Hz, 1H), 7.37 (d, *J* = 15.1 Hz, 1H), 7.30-7.23 (m, 1H), 7.18 (d, *J* = 9.1 Hz, 1H), 6.98 (s, 1H), 4.70 (dt, *J* = 47.1, 5.0 Hz, 2H), 3.82 (dt, *J* = 24.8, 5.0 Hz, 2H), 3.20 (s, 3H). ^{13}C NMR (100.6 MHz, $CDCl_3$) δ: 160.23, 156.92, 151.28, 148.87, 137.23, 132.19, 130.59, 127.91, 127.34, 127.06, 126.16, 124.38, 121.72, 120.32, 116.24, 114.26, 112.39, 106.15, 81.69 (d, $^1J_{CF}$ = 169.7 Hz), 79.86, 52.65 (d, $^2J_{CF}$ = 20.9 Hz), 39.33. HRMS: m/z calcd for $[C_{19}H_{16}FN_3 + H]^+$ 306.1401, found 306.1404.

2-((2*E*,4*E*)-5-(6-((2-fluoroethyl)(methyl)amino)naphthalen-2-yl)penta-2,4-dien-1-ylidene)malononitrile (**4c**) A black solid (25.9 mg, 65.1%) was obtained. Mp 214.1−214.9 ℃. ^{1}H NMR (400 MHz, $CDCl_3$) δ 7.74 (s, 1H), 7.72 (d, *J* = 9.2 Hz, 1H), 7.63 (d, *J* = 8.7 Hz, 1H), 7.56 (d, *J* = 9.6 Hz, 1H), 7.47 (d, *J* = 11.9 Hz, 1H), 7.14 (d, *J* = 15.2 Hz, 1H), 7.14-7.08 (m, 2H), 7.01 (dd, *J* = 15.1, 10.8 Hz, 1H), 6.93 (s, 1H), 6.84-6.75 (m, 1H), 4.68 (dt, *J* = 47.1, 5.0 Hz, 2H), 3.80 (dt, *J* = 24.6, 5.0 Hz, 2H), 3.17 (s, 3H). ^{13}C NMR (100.6 MHz, DMSO-d_6) δ: 161.94, 153.28, 148.78, 146.12, 136.37, 130.33, 130.22, 129.79, 127.22, 126.41, 126.21, 125.54, 124.59, 116.86, 115.27, 113.37, 106.00, 82.61 (d, $^1J_{CF}$ = 166.1 Hz), 77.91, 52.19 (d, $^2J_{CF}$ = 20.0 Hz), 39.16. HRMS: m/z calcd for $[C_{21}H_{18}FN_3 + H]^+$ 332.1558, found 332.1554.

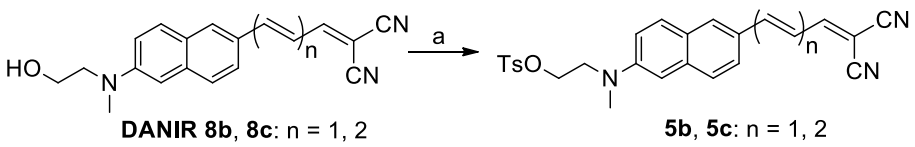

DANIR 8b, **8c**: n = 1, 2 **5b**, **5c**: n = 1, 2

Scheme S1. Reagents and conditions: (a) 4-methylbenzenesulfonic anhydride, pyridine, −20 ℃→RT, 3 d.

DANIR **8b** and **8c** were prepared by our previously reported procedures.[2]

(*E*)-2-((6-(4,4-dicyanobuta-1,3-dien-1-yl)naphthalen-2-yl)(methyl)amino)ethyl 4-methylbenzenesulfonate (**5b**) DANIR **8b** (10.0 mg, 0.033 mmol) was dissolved in 2 mL pyridine, and the solution was cooled to −20 ℃. Then 4-methylbenzenesulfonic anhydride (35.0 mg, 0.11 mmol) was added immediately, and the reaction mixture was stirred for 3 d at room temperature. After solvents were removed under vacuum, the residue was purified by column chromatography using petroleum ether/ethyl acetate (2:1, v:v) to give a dark red solid (14.3 mg, 94.7%). ^{1}H NMR (400 MHz, $CDCl_3$) δ 7.83 (s, 1H), 7.68 (d, *J* = 9.5 Hz, 1H), 7.67 (d, *J* = 8.2 Hz, 2H), 7.62-7.57 (m, 3H), 7.37 (d, *J* = 15.0 Hz, 1H), 7.30-7.23 (m, 1H), 7.18 (d, *J* = 8.1 Hz, 2H), 7.01 (dd, *J* = 9.0, 2.6 Hz, 1H), 6.74 (d, *J* = 2.2 Hz, 1H), 4.25 (t, *J* = 5.8 Hz, 2H), 3.79 (t, *J* = 5.8 Hz, 2H), 3.06 (s, 3H), 2.32 (s, 3H).

2-((6-((1*E*,3*E*)-6,6-dicyanohexa-1,3,5-trien-1-yl)naphthalen-2-yl)(methyl)amino)ethyl 4-methylbenzenesulfonate (**5c**) The same procedure as described above to prepare compound **5b** was followed, and compound **5c** was obtained as a black solid (22.0 mg, 45.5%). ^{1}H NMR (400 MHz, $CDCl_3$) δ 7.76 (s, 1H), 7.67 (d, *J* = 7.5 Hz, 2H), 7.68-7.64 (m, 1H), 7.59-7.57 (m, 2H), 7.50 (d, *J* = 12.0 Hz, 1H), 7.17 (d, *J* = 7.4 Hz, 2H), 7.18-7.11 (m, 2H), 7.06-6.85 (m, 2H), 6.81 (dd, *J* = 12.9, 12.8 Hz, 1H), 6.75 (s, 1H), 4.25 (s, 2H), 3.77 (s, 2H), 3.04 (s, 3H), 2.32 (s, 3H).

Spectroscopic Measurements. Fluorescence quantum yields were measured using a calibrated integrating sphere with a Quantaurus-QY C11347 equipment (HAMAMATSU, Japan). The increase in fluorescence intensity when FDANIR **4a-c** were activated by Aβ_{1-42} aggregates was measured by following our previously reported procedures.[3]

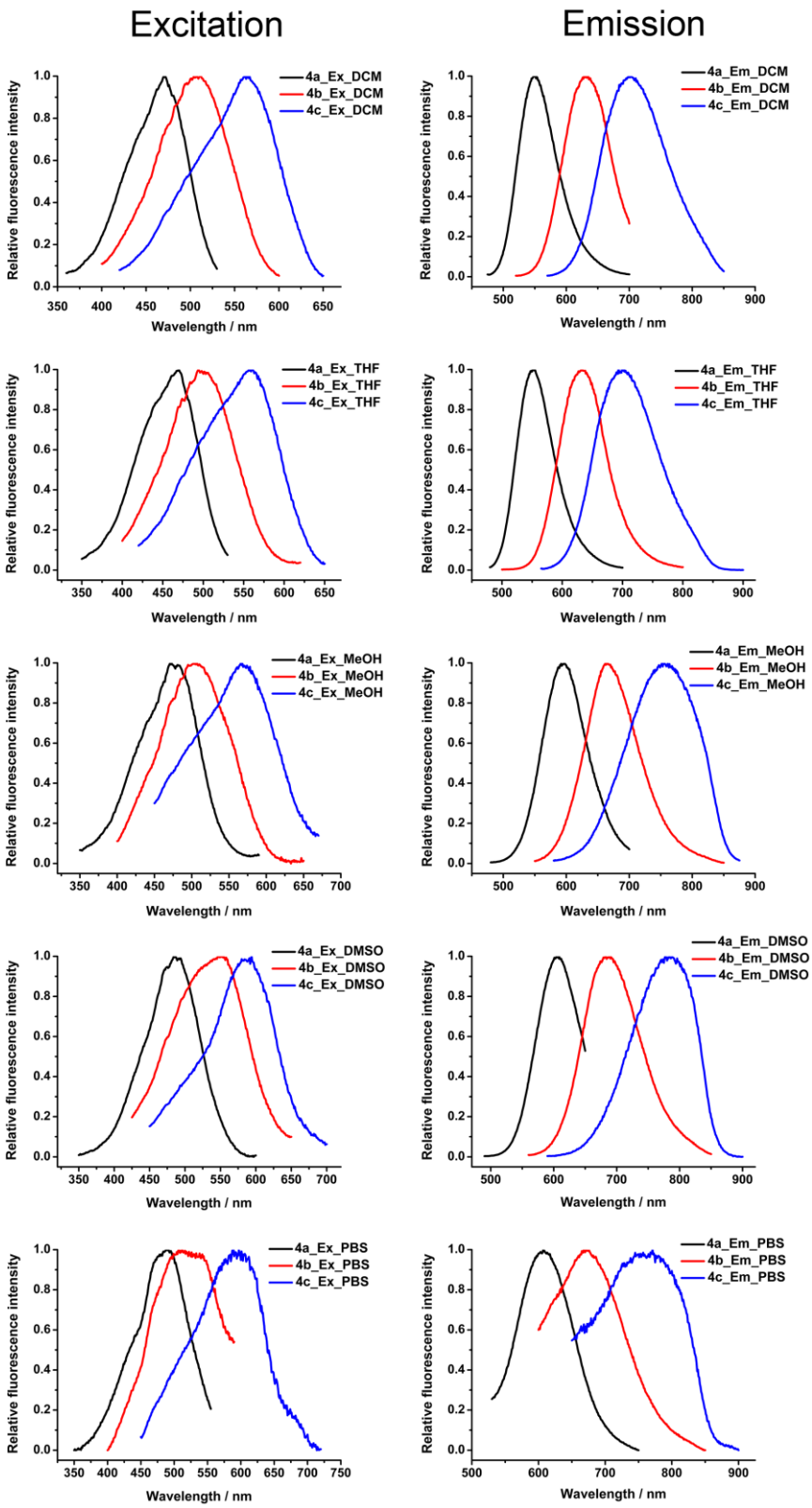

Figure S1. The excitation (left panel) and emission (right panel) spectra of the FDANIRs **4a-c** in different solvents: dichloromethane, THF, methanol, DMSO, and phosphate-buffered saline (PBS, 10% ethanol). The emission wavelengths of the solutions were measured at a concentration of 10 μM.

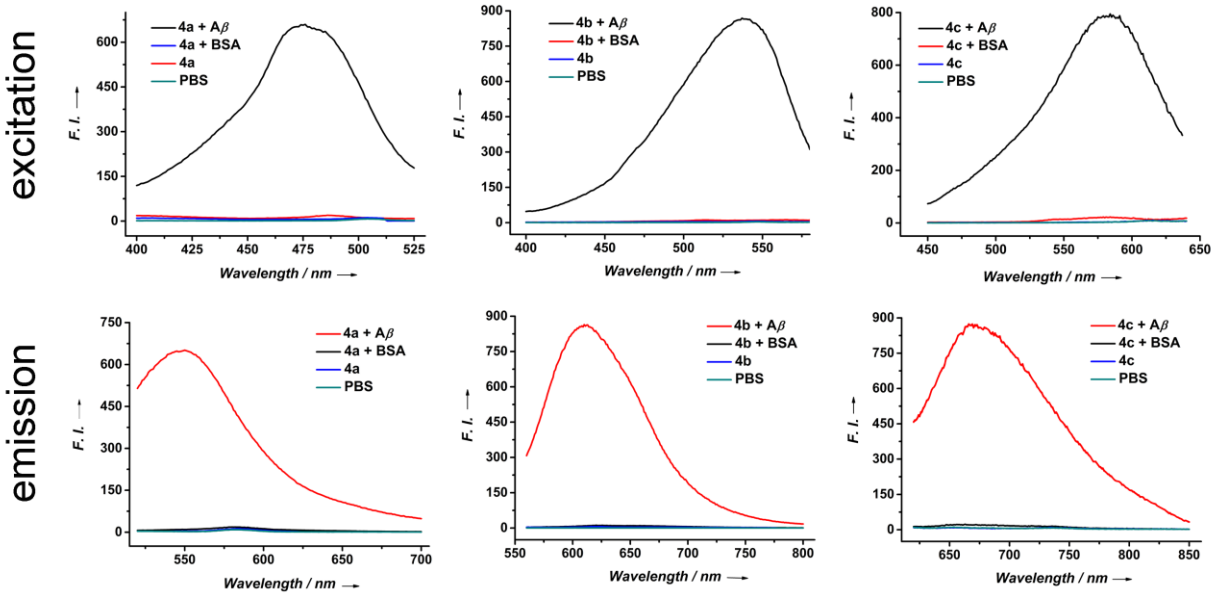

Figure S2. The excitation (top row) and emission (bottom row) spectra of the FDANIRs **4a-c** (50 nM) upon interaction with Aβ_{1-42} aggregates (10 μg/mL) or BSA (10 μg/mL). The spectra of the FDANIRs solutions in PBS (50 nM) and PBS alone were also measured under the same conditions.

Table S1. Spectroscopic properties of the FDANIR probes.

Probe	Fluorescence spectrum				UV-vis spectrum	
	Solvent	λ_{ex} nm	λ_{em} nm	Stokes shift nm	λ_{abs}[a] nm	ε[a] L mol^{-1}cm^{-1}
4a	DCM	470	549	79	462	23273
	THF	470	551	81		
	MeOH	471	597	126		
	DMSO	484	605	121		
	PBS	488	607	119		
	with Aβ	476	550	74		
4b	DCM	511	631	120	486	34540
	THF	494	633	139		
	MeOH	507	664	157		
	DMSO	552	688	136		
	PBS	512	668	156		
	with Aβ	537	610	73		
4c	DCM	562	699	137	506	40760
	THF	560	693	133		
	MeOH	566	752	186		
	DMSO	580	783	203		
	PBS	589	771	182		
	with Aβ	589	666	77		

[a] λ_{abs} and ε were measured in the solutions of dichloromethane (DCM).

In Vitro Fluorescent Staining. Paraffin-embedded 8 μm brain sections from Tg mice (C57BL6, APPswe/PSEN1, 11 months old, male) and an AD patient (male, 91 years old, M91) were used for the neuropathological staining. The staining was conducted by following the previously reported procedures.[3]

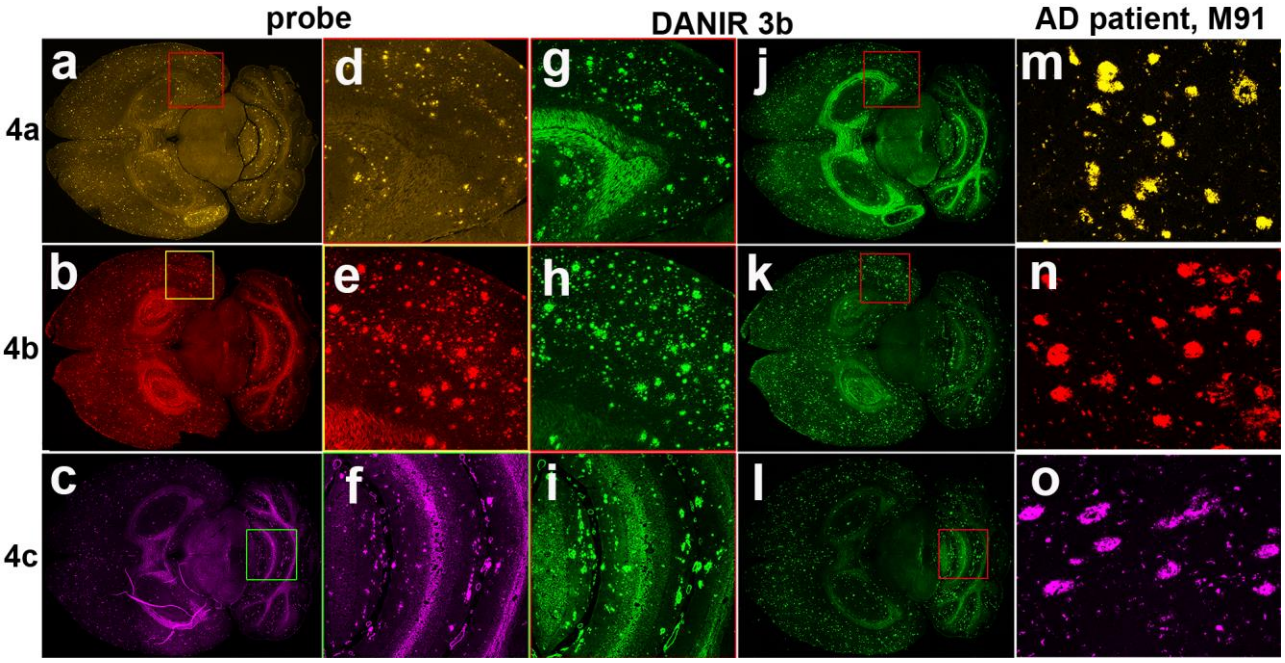

Figure S3. Histological fluorescent staining on brain sections of Tg mouse (a-l, C57BL6, APPswe/PSEN1, 11 months old, male) and an AD patient (m-o, male, 91 years old) with **4a-c**. Images of a (yellow), b (red), and c (purple) were stained with **4a-c**, respectively. The adjacent brain sections were stained with DANIR **3b** (j-l, green). Images of d-i were enlarged partial views of homologous parts of the sections. Images of m (yellow), n (red), and o (purple) were stained with **4a-c**, respectively. AF488 (**4a**), AF546 (**4b**, **4c** and DANIR **3b**) filter sets were used. Magnification, 5×.

In Vitro Saturation and Inhibition Binding Studies. In inhibition binding assays, [^{125}I]IMPY was used as competing radioligand. The saturation and inhibition binding studies of FDANIR **4a-c** were performed by following the previously reported procedures.[3]

In competition binding assays, **4a-c** showed high affinity with the values of 593.4 ± 25.0, 101.3 ± 13.2, and 11.4 ± 3.9 nM, respectively. Furthermore, the three probes inhibited the binding of [^{125}I]IMPY, the competing radioligand, in a dose-dependent manner, where the probes also showed higher affinities with the extension of the π-conjugated system (Fig. S4).

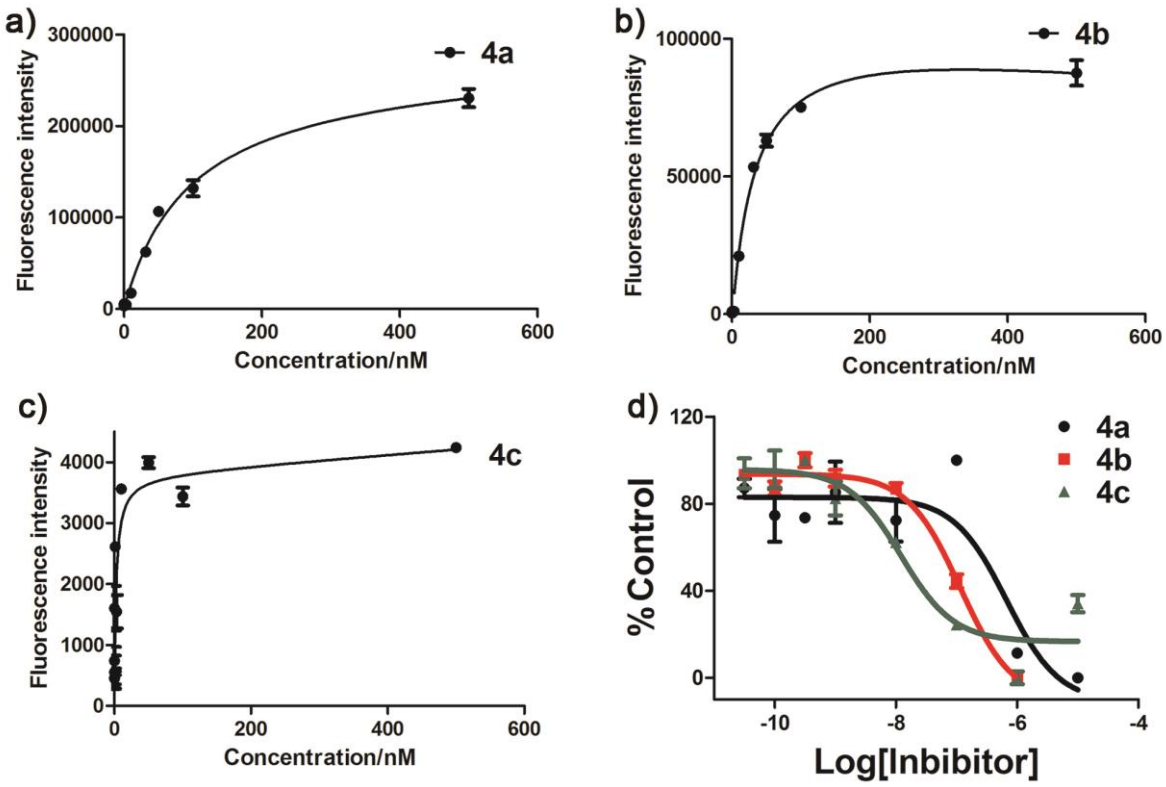

Figure S4. Plots of saturation (a-c) and inhibition (d) binding assays of FDANIR **4a-c**.

Radiolabeling.

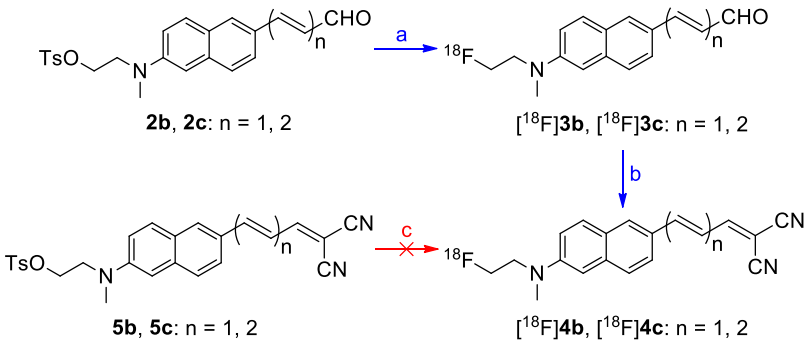

Scheme S2. Reagents and conditions: (a) Kryptofix 222, K_2CO_3, $^{18}F^-$, DMSO, 100 °C, 8 min; (b) malononitrile, K_2CO_3, ethanol, RT, 5 min; (c) Kryptofix 222, K_2CO_3, $^{18}F^-$, CH_3CN, 100 °C, 5 min.

As shown in scheme S2, we firstly used **5b** and **5c** as tosylate precursors, and tried a one-step nucleophilic substitution reaction with $^{18}F^-$ to prepare the desired ^{18}F-labeled ligands ([^{18}F]**4b** and [^{18}F]**4c**). Unfortunately, no final ^{18}F-labeled products were obtained, which may be caused by the instability of **5b** and **5c** under 100 °C in a base-catalyzed condition. As a result, a two-step strategy has to be applied and tosylate aldehydes **2b** and **2c** were used as precursors.

[^{18}F]Fluoride on the QMA cartridge was eluted into a 10 mL reaction vial with 1 mL of Kryptofix$_{222}$/K_2CO_3 solution (13 mg of Kryptofix$_{222}$ and 1.1 mg of K_2CO_3 in CH_3CN/H_2O, 4/1, v/v). The solvent was removed, and then the residue was dried azeotropically with anhydrous acetonitrile (1 mL × 3) under a stream of nitrogen at 120 ºC. The vessel was allowed to cool to room temperature, and then a solution of tosylate precursor **2b** or **2c** (2.4–3.0 mg) in anhydrous DMSO (1 mL) was added. The reaction mixture was heated to 100 ºC and kept for 8 min. After that, 10 mL of water was added, and the reaction mixture was passed through a preconditioned Sep-Pak Plus-C18 cartridge (Bonna-Agela Technologies). The cartridge was washed with 10 mL of water, and the labeled compound ([^{18}F]**3b** or [^{18}F]**3c**) was eluted to a reaction vial with ethanol (0.6 mL × 2), and the average radiochemical yields for [^{18}F]**3b** and [^{18}F]**3c** were 16% and 27% (decay corrected), respectively. Then malononitrile (0.4 mmol) was dissolved in the reaction mixture, and saturated solution of K_2CO_3 in methanol (30 μL) was added as catalyst. The reaction was kept at room temperature for 5 min, and after that, acidized with HCl (1 M, 100 μL). Finally, [^{18}F]**4b** and [^{18}F]**4c** were obtained by purifying with HPLC using a Venusil MP C18 reverse phase column (Bonna-Agela Technologies, 5 μm, 10 × 250 mm). The detailed information of radiolabeling and separation was summarized in Table S2.

Table S2. Detailed information of radiolabeling and separation.

Probe	Mobile phase CH_3CN/H_2O	Flow rate mL/min	Retention time min	UV detector nm	Total synthesis time min
[^{18}F]**4b**	65/35	4	24.9	500	87
[^{18}F]**4c**	65/35	4	37.6	510	108

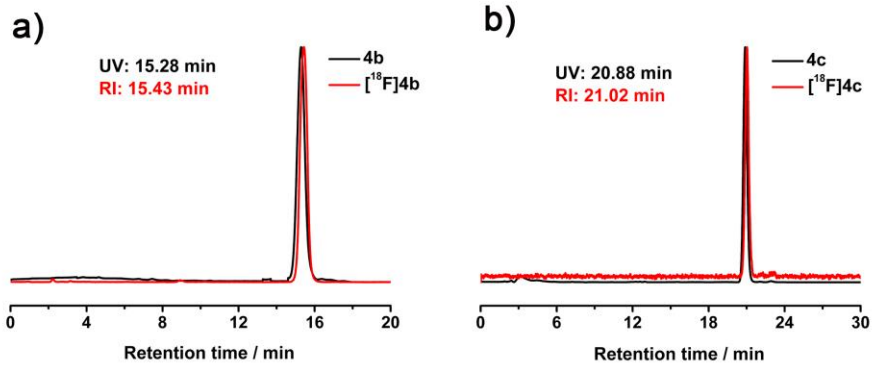

Figure S5. HPLC profiles of co-injection. HPLC conditions: Venusil MP C18 column (Bonna-Agela Technologies, 5 μm, 10 × 250 mm), CH_3CN/H_2O = 70%/30%, 4 mL/min, UV, 500 and 510 nm for **4b** and **4c**, respectively.

Biological Evaluation. Partition coefficient determination, in vitro autoradiography and in vivo biodistribution of [^{18}F]**4b** and [^{18}F]**4c** were all conducted according to previously reported methods.[4] In addition, in vivo metabolism in mice were carried out. Normal ICR mice (n = 2-3) were i.v. injected with [^{18}F]**4b** or [^{18}F]**4c** (250-500 μCi, 300 μL), and then sacrificed at 2, 10, and 30 min post-injection. Organ samples (brain, plasma and liver) and excreta (urine and feces) were collected, and the extracts were analyzed by following previously reported procedures,[5] which provided the percentage of the radioactive parent tracers and metabolites to total radioactivity (no decay corrected). Furthermore, the BBB penetration test of cold compounds **4b** and **4c** was conducted by following our previously established procedures.[6]

In Vitro Autoradiography. To characterize the specificity and high affinities of [^{18}F]**4b** and [^{18}F]**4c** to Aβ plaques, in vitro autoradiography was performed on brain sections from Tg mice (C57BL6, APPswe/PSEN1, 11 months old, male), two AD patients (female, 64 years old, F64; female, 71 years old, F71) and a cerebral amyloid angiopathy (CAA) patient (female, 68 years old, F68). As shown in Figure S6, Aβ plaques densely distribute in brain sections both from Tg mice (cortical, cerebellar and hippocampal regions) and AD/CAA patients (cortical regions), and were precisely detected by both [^{18}F]**4b** and [^{18}F]**4c**. The results were confirmed by the fluorescent staining patterns with DANIR **3b** on the same section. Furthermore, the fluorescent observation revealed that the Aβ plaques of the three AD/CAA patients existed in three different forms, including dense-core plaques (F64), diffuse plaques (F71) and the Aβ deposits within the blood vessel walls that responsible for CAA (F68). In contrast, the brain sections from WT mouse and healthy human displayed no significant accumulation of radioactivity (Figure S7). Therefore, in vitro autoradiography demonstrated that [^{18}F]**4b** and [^{18}F]**4c** have great abilities to bind with Aβ plaques in different forms, which proved their feasible and practical application in detecting Aβ plaques.

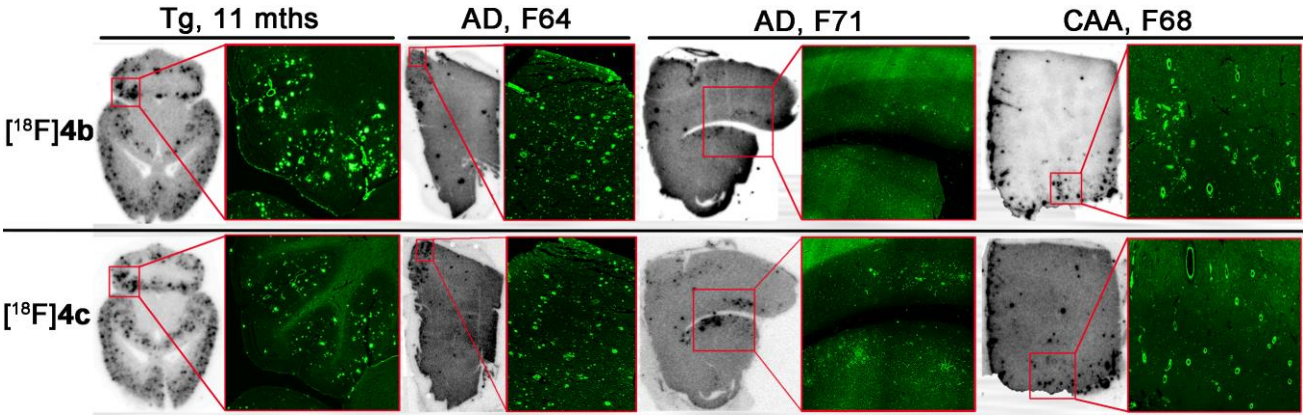

Figure S6. In vitro autoradiography of [^{18}F]**4b** (top row) and [^{18}F]**4c** (bottom row) on brain sections from Tg mice and AD/CAA patients. The presentation and distribution of plaques on the same sections were confirmed by fluorescent staining using DANIR **3b** (green images of the right panels).

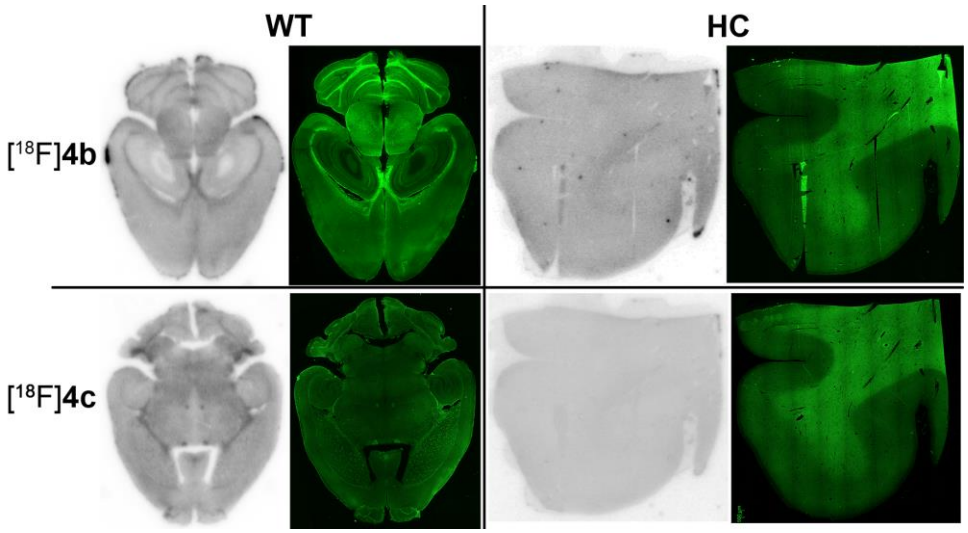

Figure S7. In vitro autoradiography of [^{18}F]**4b** (top row) and [^{18}F]**4c** (bottom row) on brain sections of WT mice (left panel) and health control (HC) human (male, 84 years old, right panel). The results was confirmed by staining the same sections with DANIR **3b**.

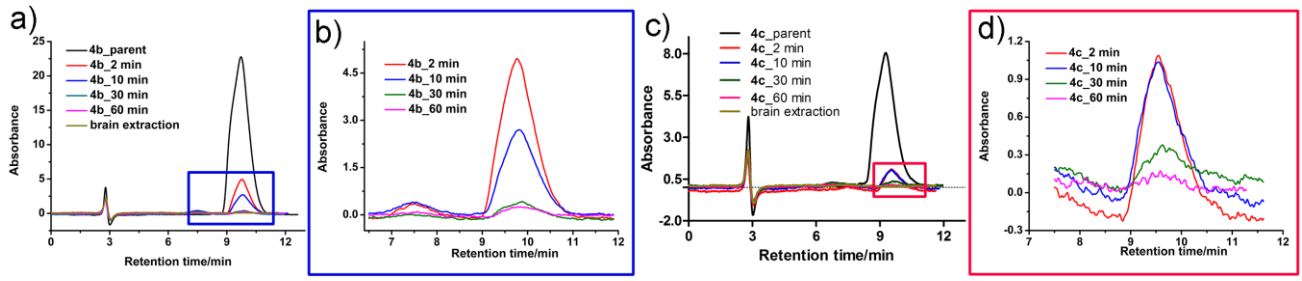

Figure S8. HPLC profiles of brain extraction at different time points after i.v. injection of **4b** (a) and **4c** (c). (b) and (d) are enlarged partial views of the peaks. HPLC conditions: Cosmosil packed column (5C18-AR-II, 4.6 × 150 mm); for **4b**: CH_3CN/H_2O = 60%/40%, 1 mL/min, UV, 500 nm; for **4c**: CH_3CN/H_2O = 70%/30%, 1 mL/min, UV, 510 nm.

Table S3. Brain uptakes of [^{18}F]4b, [^{18}F]4c, 4b and 4c at different time points

probe	brain uptake/% ID/g				$brain_{10min}/brain_{60min}$
	2 min	10 min	30 min	60 min	
4b	10.97 ± 1.09	6.16 ± 0.30	2.63 ± 0.19	0.71 ± 0.09	15.5
4c	6.88 ± 0.47	5.08 ± 0.74	2.11 ± 0.37	1.03 ± 0.07	6.7

In Vivo Biodistribution.

Table S4. Biodistribution of radioactivity after i.v. injection of [^{18}F]**4b** and [^{18}F]**4c**.[a]

organ	uptake/% ID/g			
	2 min	10 min	30 min	60 min
	[^{18}F]**4b** (log *D* = 2.82 ± 0.57)			
blood	4.83 ± 0.28	4.95 ± 0.23	5.53 ± 0.30	6.22 ± 0.032
brain	**5.04 ± 0.46**	**5.29 ± 0.33**	**4.21 ± 0.44**	**3.85 ± 0.24**
heart	10.52 ± 1.15	5.57 ± 0.30	4.82 ± 0.21	5.24 ± 0.41
liver	27.09 ± 2.48	16.39 ± 0.89	9.13 ± 0.45	7.82 ± 0.90
spleen	10.25 ± 2.79	5.71 ± 0.23	4.33 ± 0.35	4.23 ± 0.47
lung	9.45 ± 1.27	6.16 ± 0.32	5.25 ± 0.20	5.16 ± 0.094
kidney	14.45 ± 0.68	7.82 ± 0.35	5.34 ± 0.39	4.71 ± 0.42
pancreas	8.73 ± 2.40	5.27 ± 0.38	3.58 ± 0.33	3.31 ± 0.46
muscle	4.47 ± 0.46	4.38 ± 0.45	3.86 ± 0.31	3.92 ± 0.54
bone	2.90 ± 0.43	3.58 ± 0.34	4.68 ± 0.50	9.70 ± 0.95
stomach[b]	1.18 ± 0.20	1.41 ± 0.26	1.51 ± 0.21	1.59 ± 0.31
small intestine[b]	5.53 ± 0.77	9.38 ± 1.05	12.70 ± 0.94	18.04 ± 2.41
	[^{18}F]**4c** (log *D* = 3.41 ± 0.047)			
blood	4.01 ± 0.17	3.01 ± 0.20	3.58 ± 0.17	3.69 ± 0.25
brain	**3.00 ± 0.12**	**4.26 ± 0.60**	**3.83 ± 0.31**	**3.01 ± 0.34**
heart	13.65 ± 0.90	4.91 ± 0.32	4.08 ± 0.34	3.96 ± 0.90
liver	36.84 ± 3.86	17.51 ± 1.66	9.46 ± 0.57	6.68 ± 0.60
spleen	10.78 ± 1.44	6.02 ± 1.02	3.80 ± 0.24	3.13 ± 0.30
lung	10.10 ± 1.01	4.94 ± 0.62	3.99 ± 0.33	3.86 ± 0.36
kidney	15.35 ± 1.10	7.84 ± 0.74	5.45 ± 0.39	4.06 ± 0.41
pancreas	6.40 ± 0.38	4.87 ± 0.34	3.45 ± 0.38	3.02 ± 0.28
muscle	4.13 ± 0.43	3.44 ± 0.34	3.32 ± 0.13	2.95 ± 0.68
bone	2.93 ± 0.44	2.45 ± 0.54	4.99 ± 1.01	7.23 ± 0.61
stomach[b]	1.04 ± 0.19	1.58 ± 0.57	1.84 ± 0.66	1.51 ± 0.18
small intestine[b]	4.25 ± 0.68	11.44 ± 1.09	25.79 ± 2.09	31.16 ± 2.43

[a]Each value represents the mean ± SD for 4-5 mice.

[b]Expressed as % injected dose per organ.

We may attribute the differences in brain kinetics to measuring means. That is to say, in the biodistribution experiments of [^{18}F]**4b** and [^{18}F]**4c**, the radioactivity was characterized by the "total counts" measured with a γ-counter, which included the signals from both parent compounds and

radio-metabolites; but conversely, in measuring the brain uptake of **4b** and **4c**, an HPLC device was used, and the brain uptake values were calculated from the peak areas derived from HPLC profiles, which only reflected the signals of parent compounds (Figure S8).

In Vivo Metabolism. To further understand the pharmacokinetics of [^{18}F]**4b** and [^{18}F]**4c**, we conducted in vivo metabolism experiments in ICR mice (male, 5 weeks) at different time points of 2, 10 and 30 min. Table S5 summarized the detailed information of radioactive metabolites. In brain, two radioactive metabolites were observed after dosing each of [^{18}F]**4b** and [^{18}F]**4c**, and they displayed good biostability with 68.4% and 74.8% of parent tracers left at 2 min post-injection, respectively, but steadily dropped to 27.1% and 11.5% at 30 min, respectively. In plasma, [^{18}F]**4b** was rapidly metabolized and only 29.7% of intact tracer at 2 min post-injection was left. Similarly, [^{18}F]**4c** was more extensively degraded with only 1.6% of parent remained at 10 min. For both, no parent tracers were found at 30 min post-injection in plasma, and all of the detected radioactivity was determined to be polar metabolites with the shortest retention times of approximately 2 min. In liver, [^{18}F]**4b** exhibited good biostability, and the intact [^{18}F]**4b** occupied 30.2% of total radioactivity at 30 min post-injection. Consistent with the results in plasma, [^{18}F]**4c** displayed a faster metabolism in liver, and the percentage of unmetabolized [^{18}F]**4c** decreased to 12.7% at 30 min.

Table S5. Percentages and retention times (RTs)[a] of metabolites extracted from the brain, plasma, liver, urine and feces of ICR mice after intravenous injection of [^{18}F]**4b** and [^{18}F]**4c**.[b]

probe	organ	post-injection time (min)	[^{18}F]**4b-1** (%) RT = 2.3 min	[^{18}F]**4b-2** (%) RT = 7.2 min	[^{18}F]**4b** (%) RT = 11.2 min
[^{18}F]**4b**	brain	2	23.3 ± 4.1	8.3 ± 1.8	68.4 ± 2.2
		10	32.2 ± 6.7	14.0 ± 4.1	53.8 ± 3.1
		30	61.4 ± 4.9	11.5 ± 4.1	27.1 ± 0.8
	plasma	2	70.3 ± 1.6	-	29.7 ± 1.6
		10	81.2 ± 1.9	-	18.8 ± 1.9
		30	100	-	-
	liver	2	35.1 ± 8.9	-	64.9 ± 8.9
		10	14.8 ± 3.6	-	85.2 ± 1.9
		30	69.8 ± 9.3	-	30.2 ± 9.3
	urine	2	-	-	-
		10	100	-	-
		30	100	-	-
	feces	2	-	-	-
		10	100	-	-
		30	100	-	-
			[^{18}F]**4c-1** (%) RT = 2.2 min	[^{18}F]**4c-2** (%) RT = 7.2 min	[^{18}F]**4c** (%) RT = 10.9 min
[^{18}F]**4c**	brain	2	25.2 ± 6.5	-	74.8 ± 6.4
		10	63.7 ± 6.8	11.3 ± 3.1	25.0 ± 3.7
		30	75.6 ± 4.9	12.9 ± 2.5	11.5 ± 2.4
	plasma	2	48.8 ± 5.9	-	51.2 ± 5.9
		10	98.4 ± 1.6	-	1.6 ± 1.6
		30	100	-	-
	liver	2	12.7 ± 2.0	11.2 ± 0.5	76.1 ± 2.6
		10	46.6 ± 6.1	10.0 ± 2.9	43.4 ± 3.4
		30	87.3 ± 1.4	-	12.7 ± 1.4
	urine	2	-	-	-
		10	100	-	-
		30	100	-	-
	feces	2	-	-	-
		10	100	-	-
		30	100	-	-

[a]HPLC conditions: Cosmosil packed column (5C18-AR-II, 4.6 × 150 mm); for **4b**: CH_3CN/H_2O = 60%/40%, 1 mL/min, UV, 500 nm; for **4c**: CH_3CN/H_2O = 65%/35%, 1 mL/min, UV, 510 nm.

[b]Each value represents the mean ± SD for 2-3 mice at each interval.

In Vivo NIR Imaging. Nude mice (BALB/c nude, 6 weeks, female), Tg mice (n = 3, C57BL6, APPsw/PSEN1, 22 months old, female) and age-matched WT mice (n = 4, C57BL6, 22 months old, female) were used for in vivo NIR imaging of **4b** and **4c** (0.2 mg/kg, 15% DMSO, 85% propylene glycol, 50 μL). The imaging was performed on an IVIS Lumina III system (PerkinElmer, the USA) with proper filter sets (Table S6). The fluorescence signals from brain were collected and analyzed by following our previously reported procedures.[3]

Table S6. Details of filter sets.

probe	mice type	filter sets	
		ex/nm	em/nm
4b	nude	520	670
4c	nude	580	790
	Tg	580	670
	WT	580	670

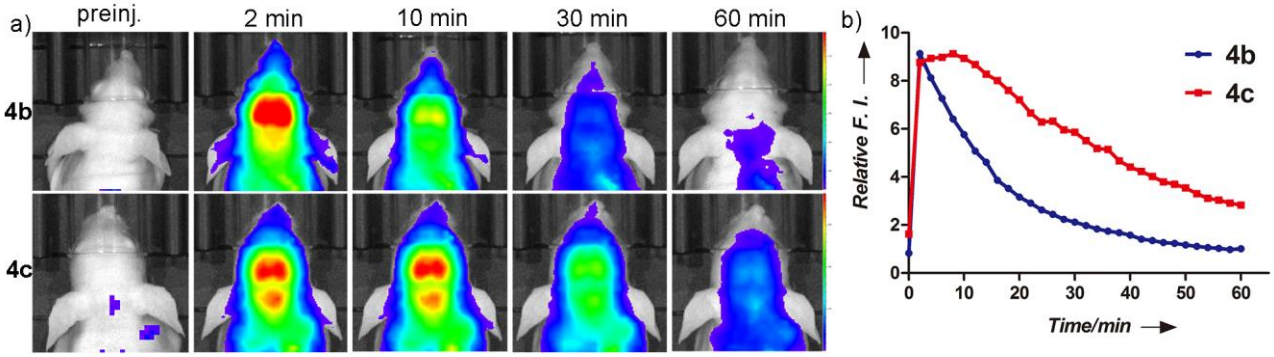

Figure S9. (a) In vivo NIR imaging images of nude mice at different time points before and after i.v. injection of **4b** (top row) and **4c** (bottom row). (b) Brain clearance curves of **4b** (blue line) and **4c** (red line) in nude mice.

Ex Vivo Histology. A Tg mouse (C57BL6, APPsw/PSEN1, 22 months old, female) and an age-matched WT mouse (C57BL6, 22 months old, female) were i.v. injected with **4c** (0.2 mg/kg, 15% DMSO, 85% propylene glycol, 50 μL) and sacrificed at 20 min after injection. We prepared frozen sections and conducted fluorescent microscopy following previously reported protocols.[3]

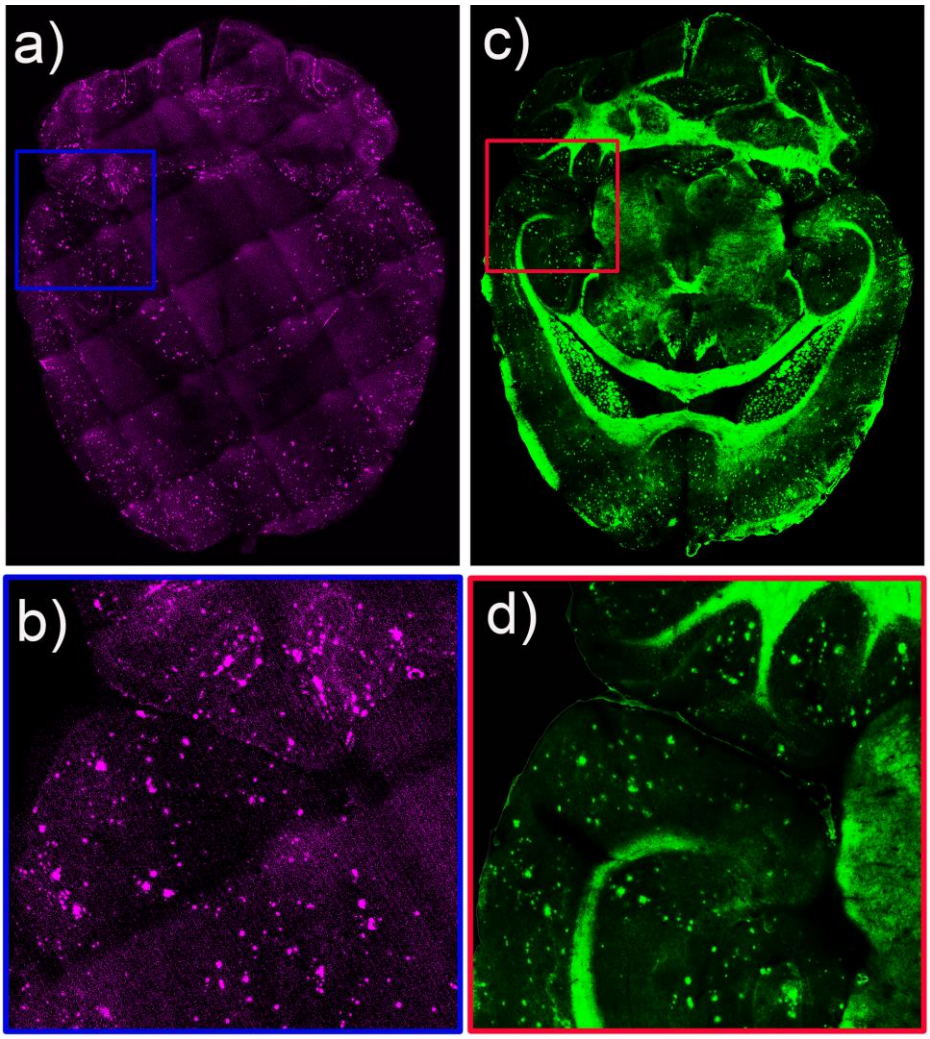

Figure S10. Ex vivo histology results of Tg mice brain slices containing cortical, cerebellar and hippocampal regions after i.v. injection of **4c** (a). The Aβ plaques were confirmed by staining the same sections with Th-S (c). Images b and d are partial enlarged views of homologous sections.

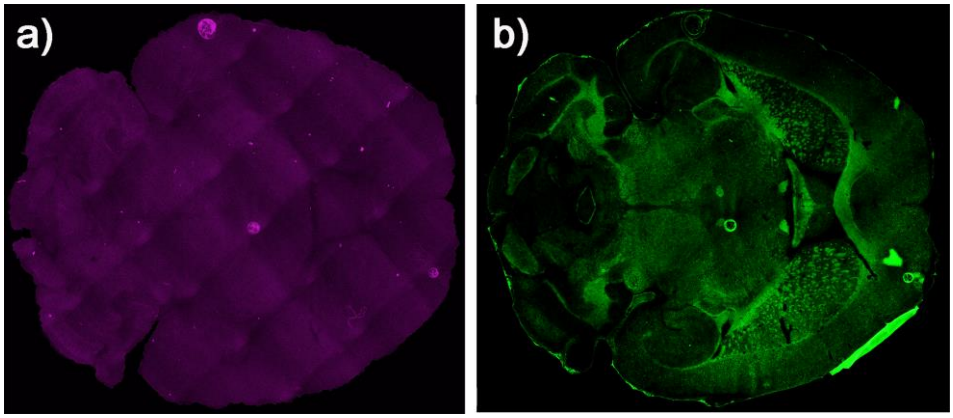

Figure S11. (a) Ex vivo histological staining of the brain sections from WT mouse. The microscope observation result was also confirmed by the staining the same section with Th-S (b).

Determination of Cerenkov Efficiency. The Cerenkov efficiency was measured with an IVIS Lumina III system (PerkinElmer, the USA). The radiotracers [^{18}F]**4b** and [^{18}F]**4c** were diluted with water into different concentrations (radioactivity). Aliquots of 300 μL aqueous solution with the radiotracer ([^{18}F]**4b** or [^{18}F]**4c**) were placed in each well of black 96-well Costar assay plates in triplicate for each concentration. Images were acquired with open filter over an exposure time of 100 s (f = 1, bin = 8). Wavelength-resolved spectral images were obtained using a series of narrow emission filter sets (520−845 nm). Cerenkov signal was normalized to photons per second per centimeter square per steradian (p/s/cm^2/sr) and analyzed with Living Image software 4.5.3 (PerkinElmer, the USA).

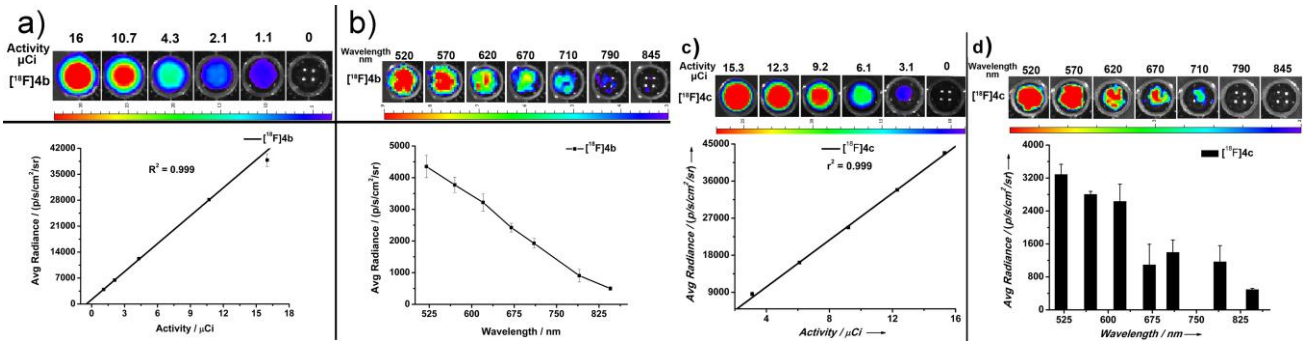

Figure S12. (a and c) Optical images of [^{18}F]**4b** (a) and [^{18}F]**4c** (c) detected with different amount of radioactivity (top row), and correlation of the optical signals and radioactivity (r^2 = 0.999, bottom row). (b and d) Optical images derived with various narrow filters for [^{18}F]**4b** (b) and [^{18}F]**4c** (d) with fixed radioactivity (top row) and its schematic (bottom row).

In Vivo Cerenkov Luminescence Imaging. For in vivo CLI, the same animals as for NIR imaging of **4c** were used. After scalp hair removed, mice were i.v. injected with [^{18}F]**4c** (200 μCi), and the acquisition of CLI signal in brain compartment was performed (open filter, f = 1, bin = 8, and exposure time = 100 s) immediately over a time course of 90 min. During this, the mice were under anesthesia with 2.5% isoflurane gas in an oxygen flow of 0.8 L/min. After the images were normalized to photons per second per centimeter square per steradian (p/s/cm^2/sr), the same region of interest (ROI) as for NIR imaging was draw with the area around the brain region, and the brain clearance curves were obtained by following the same method that was used for NIR imaging of **4c**. The CLI images were not decay corrected for all quantification because our comparisons between different animal groups were made at the same time points, and under the same acquisition parameters.

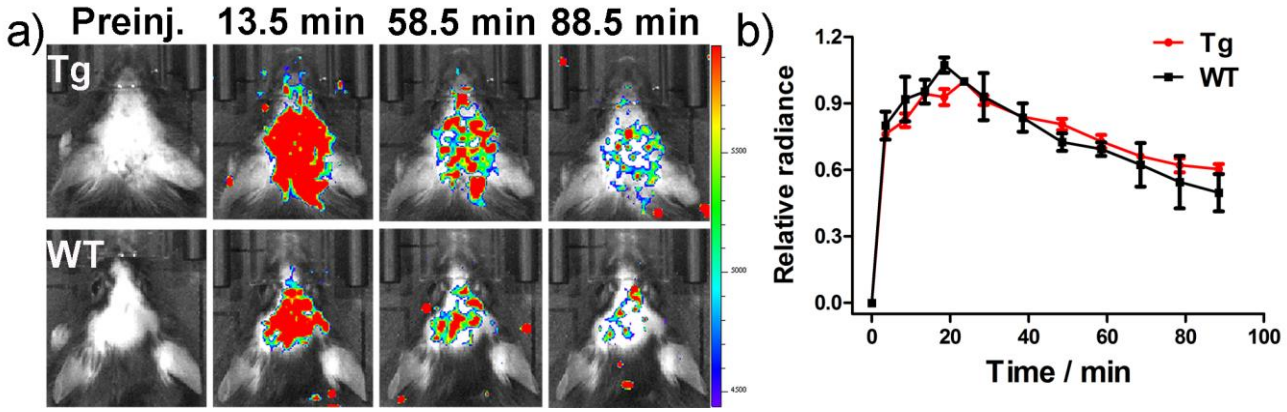

Figure S13. (a) CLI images of Tg (top row) and WT (bottom row) mice at different time points post-injection. (b) Brain clearance curves derived from CLI.

Appendixes: ^{1}H-NMR, ^{13}C-NMR, MS, and HRMS

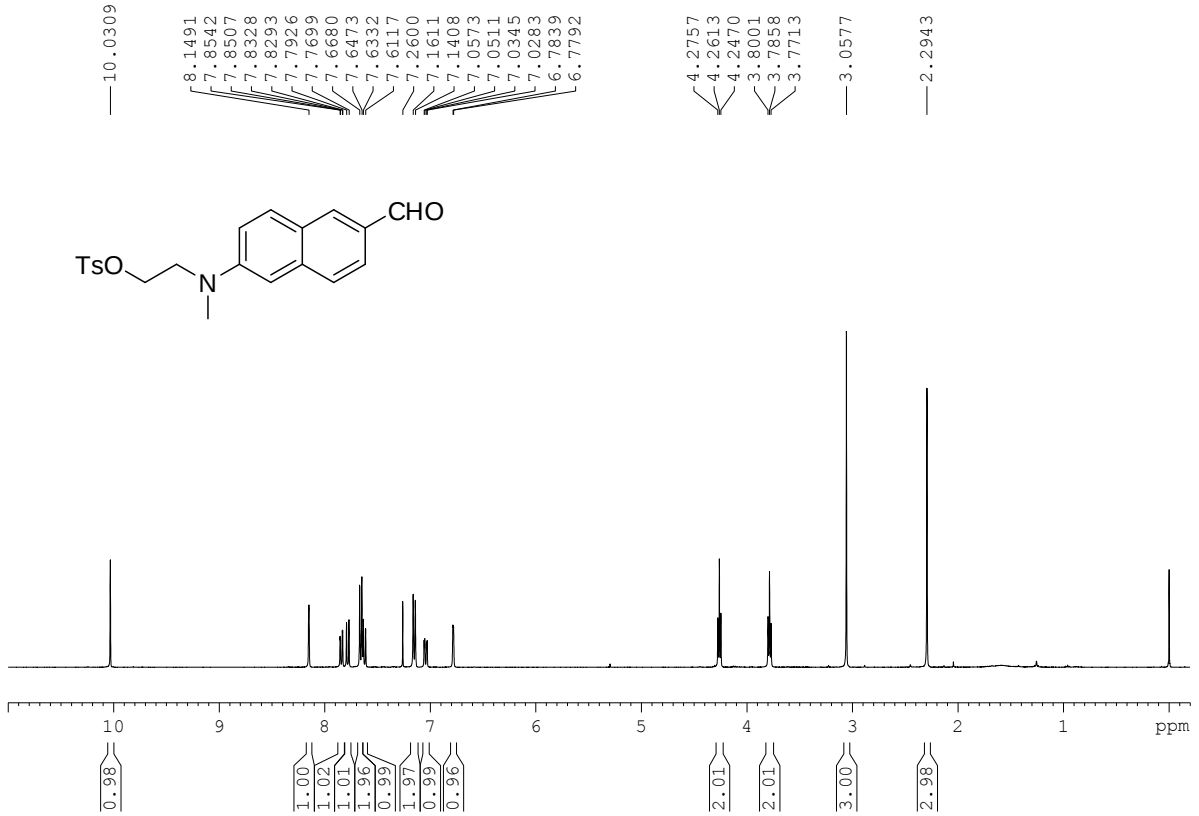

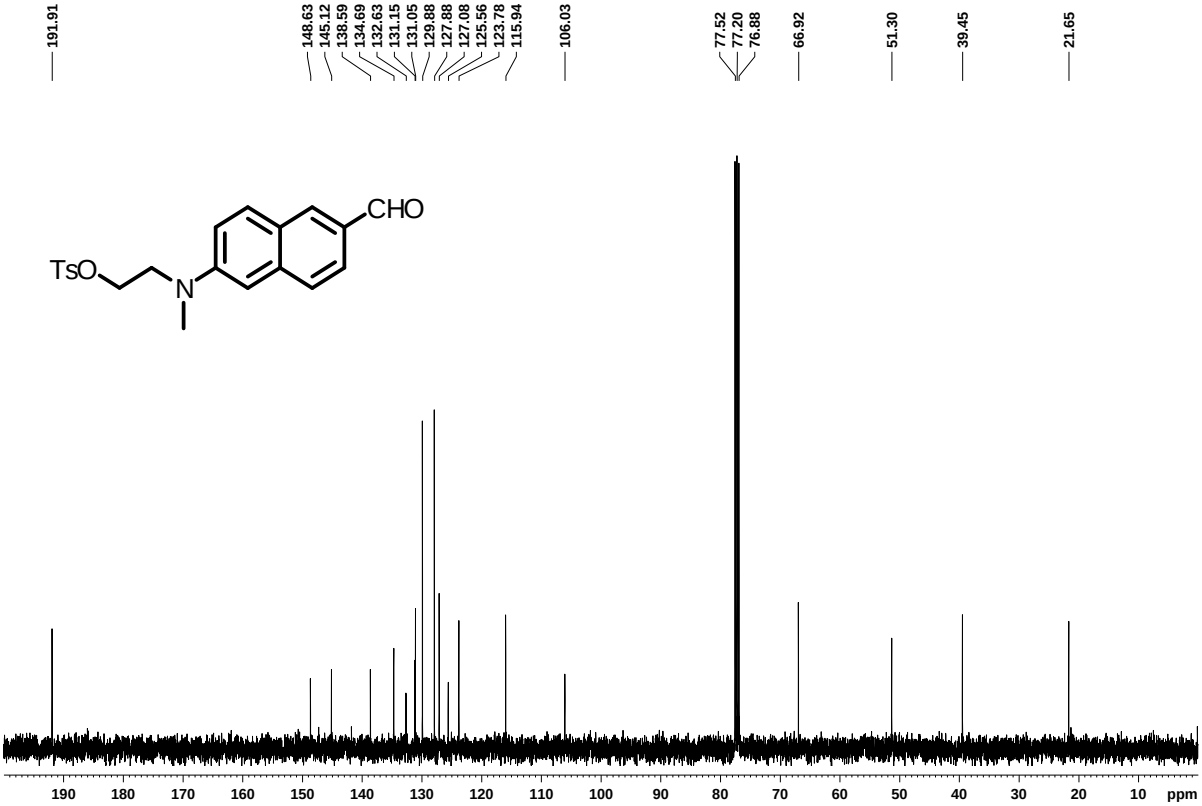

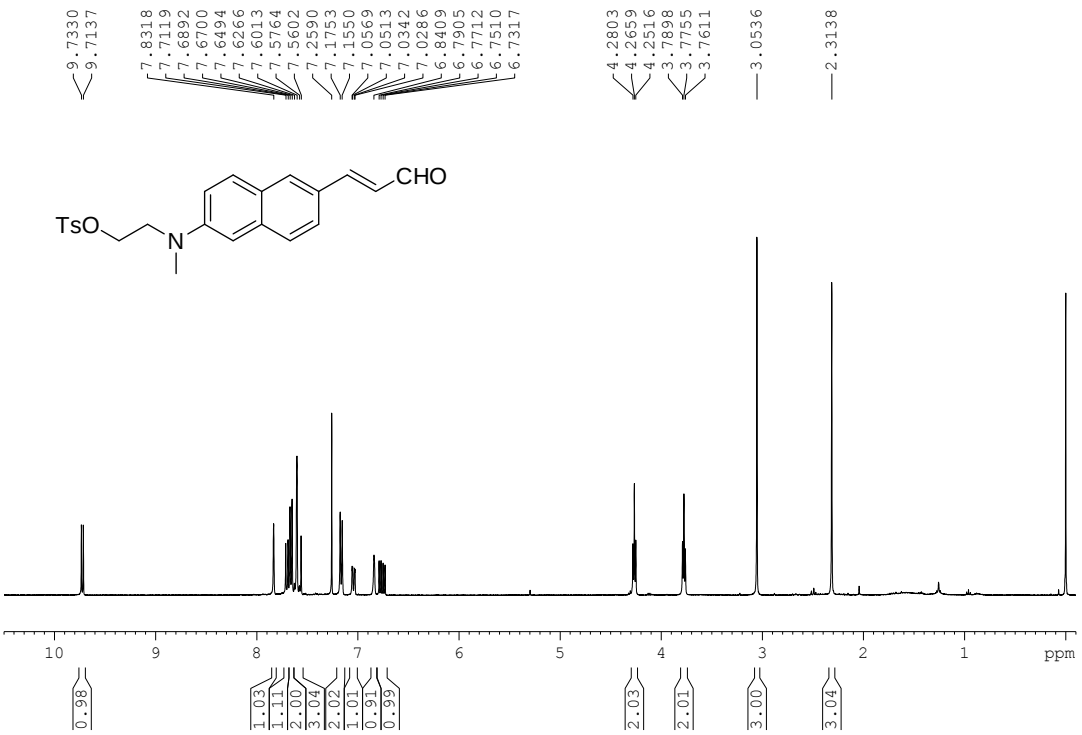
9.7330
9.7137
7.8318
7.7119
7.6892
7.6700
7.6494
7.6266
7.6013
7.5764
7.5602
7.2590
7.1753
7.1550
7.0569
7.0513
7.0342
7.0286
6.8409
6.7905
6.7712
6.7510
6.7317
4.2803
4.2659
4.2516
3.7898
3.7755
3.7611
3.0536
2.3138
CHO
TsO
N
10
9
8
7
6
5
4
3
2
1
ppm
0.98
1.03
1.11
2.00
3.04
2.02
1.01
0.91
0.99
2.03
2.01
3.00
3.04

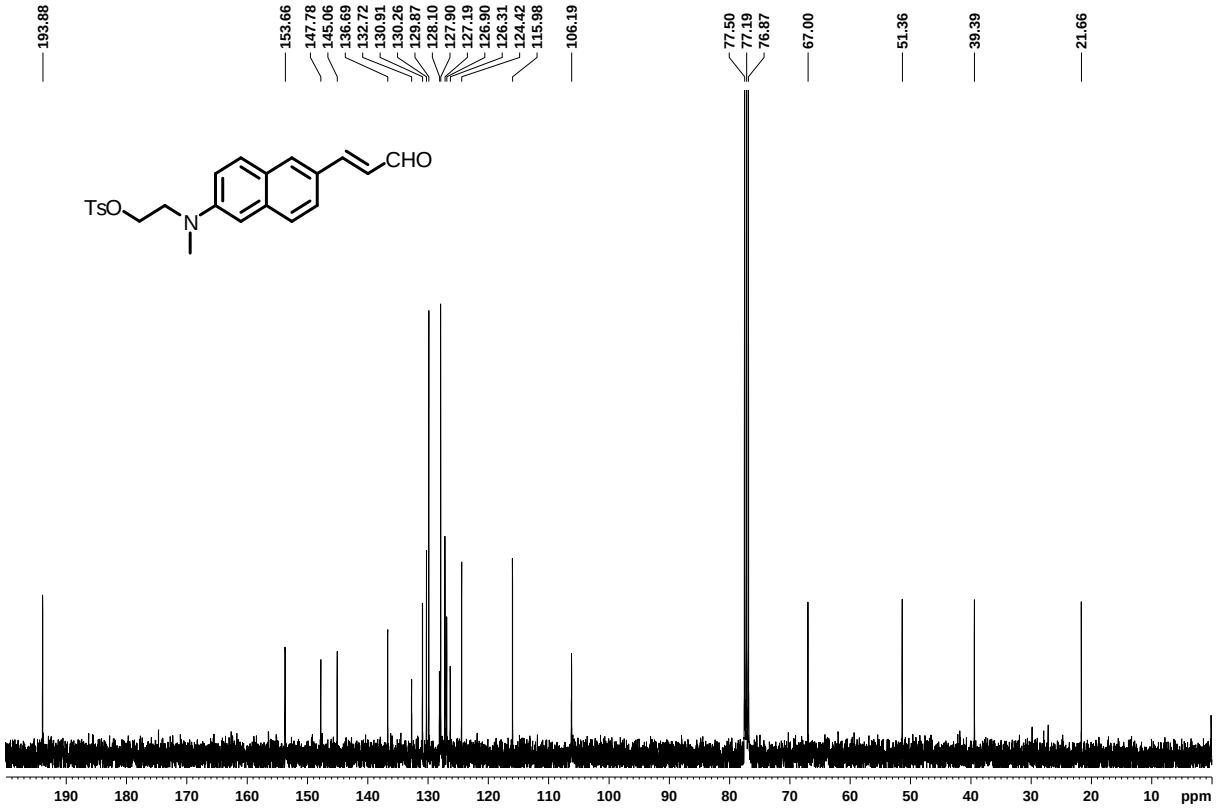
193.88
153.66
147.78
145.06
136.69
132.72
130.91
130.26
129.87
128.10
127.90
127.19
126.90
126.31
124.42
115.98
106.19
77.50
77.19
76.87
67.00
51.36
39.39
21.66
CHO
TsO
N
190
180
170
160
150
140
130
120
110
100
90
80
70
60
50
40
30
20
10
ppm

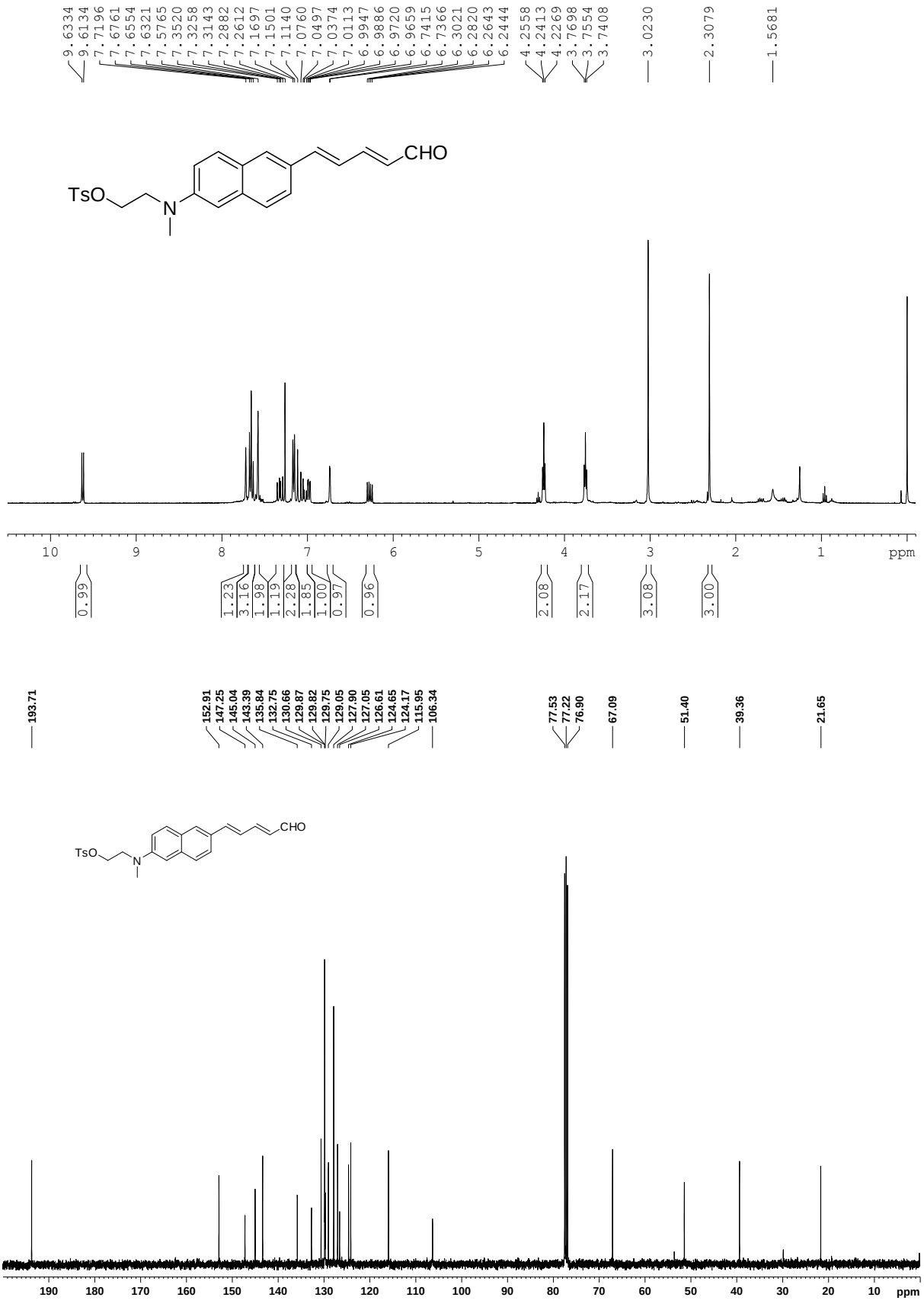
9.6334
9.6134
7.7196
7.6761
7.6554
7.6321
7.5765
7.3520
7.3258
7.3143
7.2882
7.2612
7.1697
7.1501
7.1140
7.0760
7.0497
7.0374
7.0113
6.9947
6.9886
6.9720
6.9659
6.7415
6.7366
6.3021
6.2820
6.2643
6.2444
4.2558
4.2413
4.2269
3.7698
3.7554
3.7408
3.0230
2.3079
1.5681
CHO
TsO
N
10
9
8
7
6
5
4
3
2
1
ppm
0.99
1.23
3.16
1.98
1.19
2.28
1.85
1.00
0.97
0.96
2.08
2.17
3.08
3.00
193.71
152.91
147.25
145.04
143.39
135.84
132.75
130.66
129.87
129.82
129.75
129.05
127.90
127.05
126.61
124.65
124.17
115.95
106.34
77.53
77.22
76.90
67.09
51.40
39.36
21.65
CHO
TsO
N
190
180
170
160
150
140
130
120
110
100
90
80
70
60
50
40
30
20
10
ppm

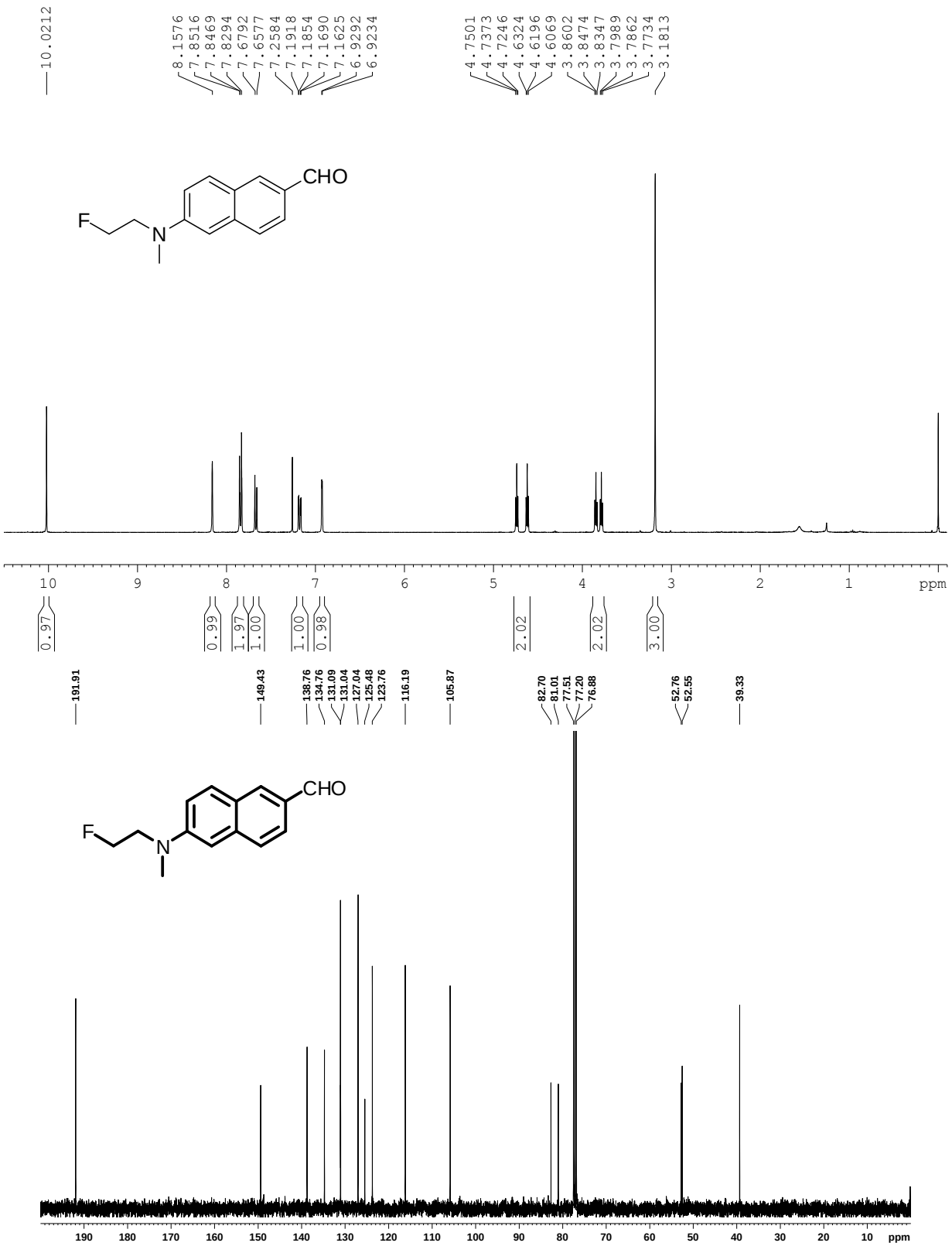
10.0212
8.1576
7.8516
7.8469
7.8294
7.6792
7.6577
7.2584
7.1918
7.1854
7.1690
7.1625
6.9292
6.9234
4.7501
4.7373
4.7246
4.6324
4.6196
4.6069
3.8602
3.8474
3.8347
3.7989
3.7862
3.7734
3.1813
CHO
F
N
10
9
8
7
6
5
4
3
2
1
ppm
0.97
0.99
1.97
1.00
1.00
0.98
2.02
2.02
3.00
191.91
149.43
138.76
134.76
131.09
131.04
127.04
125.48
123.76
116.19
105.87
82.70
81.01
77.51
77.20
76.88
52.76
52.55
39.33
CHO
F
N
190
180
170
160
150
140
130
120
110
100
90
80
70
60
50
40
30
20
10
ppm

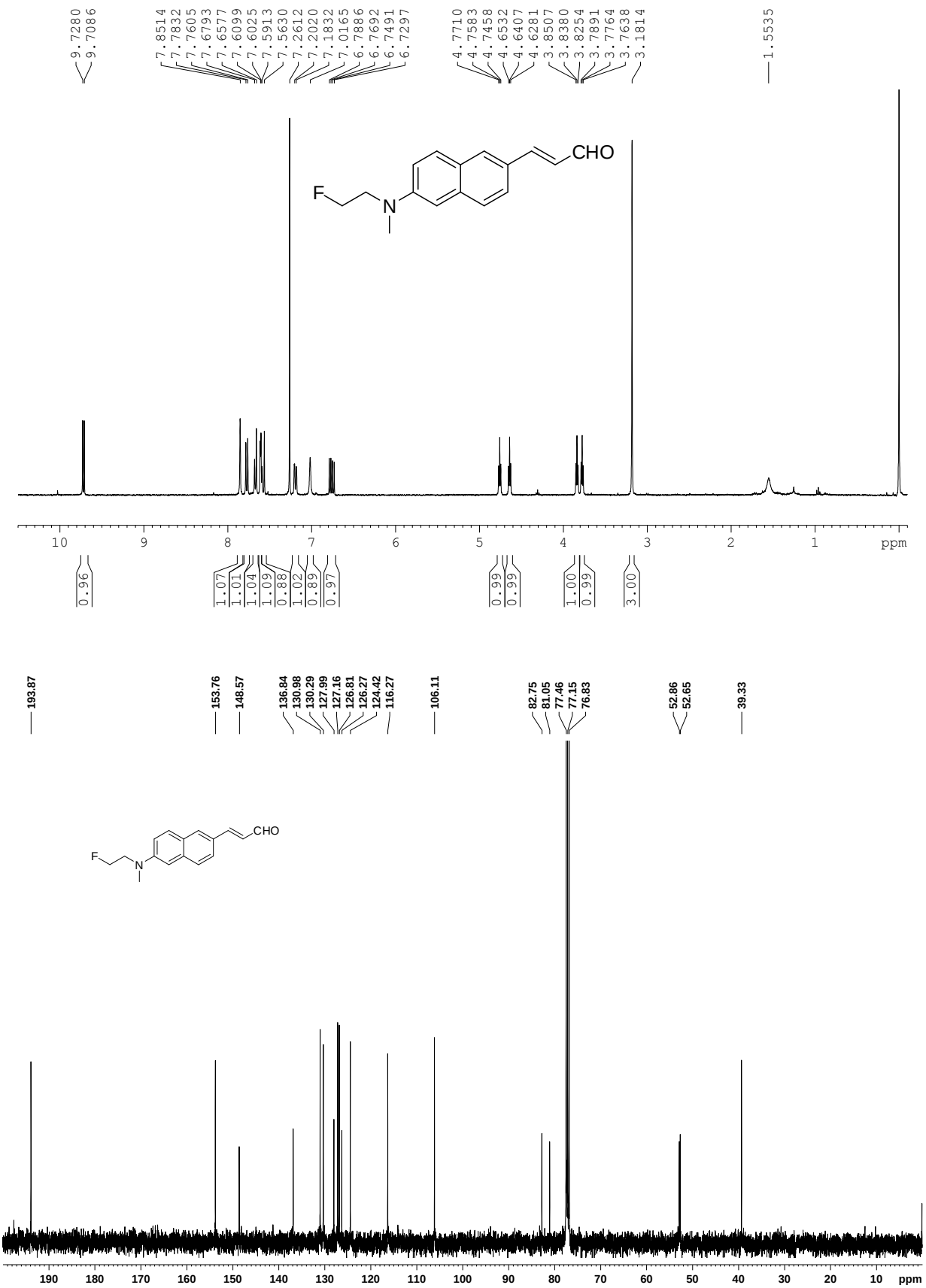
9.7280
9.7086
7.8514
7.7832
7.7605
7.6793
7.6577
7.6099
7.6025
7.5913
7.5630
7.2612
7.2020
7.1832
7.0165
6.7886
6.7692
6.7491
6.7297
4.7710
4.7583
4.7458
4.6532
4.6407
4.6281
3.8507
3.8380
3.8254
3.7891
3.7764
3.7638
3.1814
1.5535
CHO
F
N
ppm
0.96
1.07
1.01
1.04
1.09
0.88
1.02
0.89
0.97
0.99
0.99
1.00
0.99
3.00
193.87
153.76
148.57
136.84
130.98
130.29
127.99
127.16
126.81
126.27
124.42
116.27
106.11
82.75
81.05
77.46
77.15
76.83
52.86
52.65
39.33
CHO
F
N
ppm

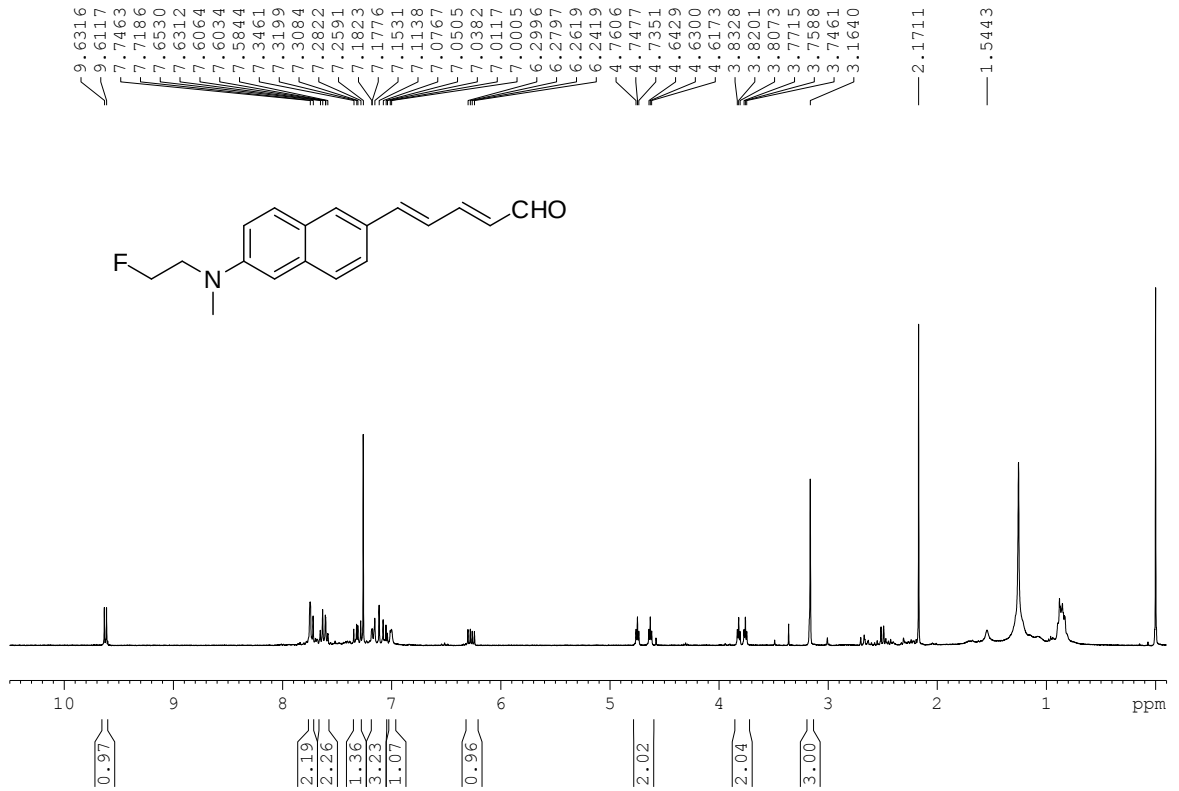
9.6316
9.6117
7.7463
7.7186
7.6530
7.6312
7.6064
7.6034
7.5844
7.3461
7.3199
7.3084
7.2822
7.2591
7.1823
7.1776
7.1531
7.1138
7.0767
7.0505
7.0382
7.0117
7.0005
6.2996
6.2797
6.2619
6.2419
4.7606
4.7477
4.7351
4.6429
4.6300
4.6173
3.8328
3.8201
3.8073
3.7715
3.7588
3.7461
3.1640
2.1711
1.5443
CHO
F
N
10
9
8
7
6
5
4
3
2
1
ppm
0.97
2.19
2.26
1.36
3.23
1.07
0.96
2.02
2.04
3.00

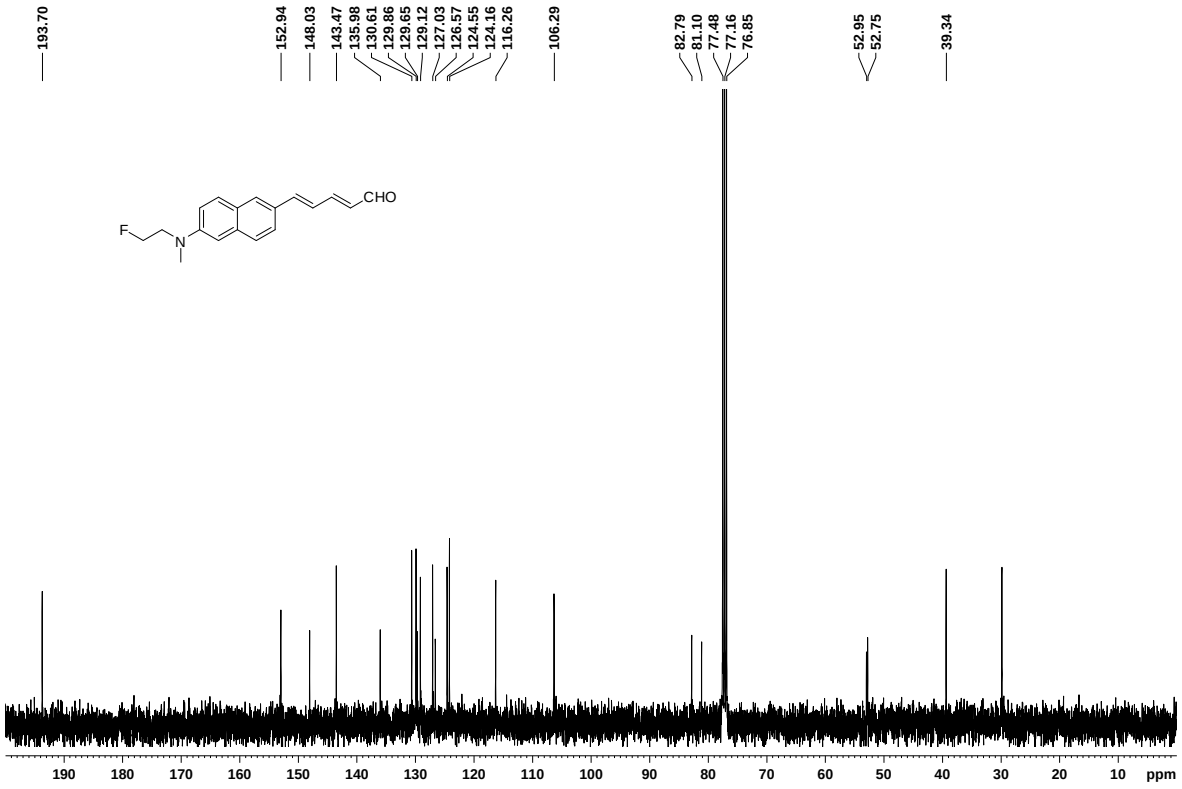
193.70
152.94
148.03
143.47
135.98
130.61
129.86
129.65
129.12
127.03
126.57
124.55
124.16
116.26
106.29
82.79
81.10
77.48
77.16
76.85
52.95
52.75
39.34
CHO
F
N
190
180
170
160
150
140
130
120
110
100
90
80
70
60
50
40
30
20
10
ppm

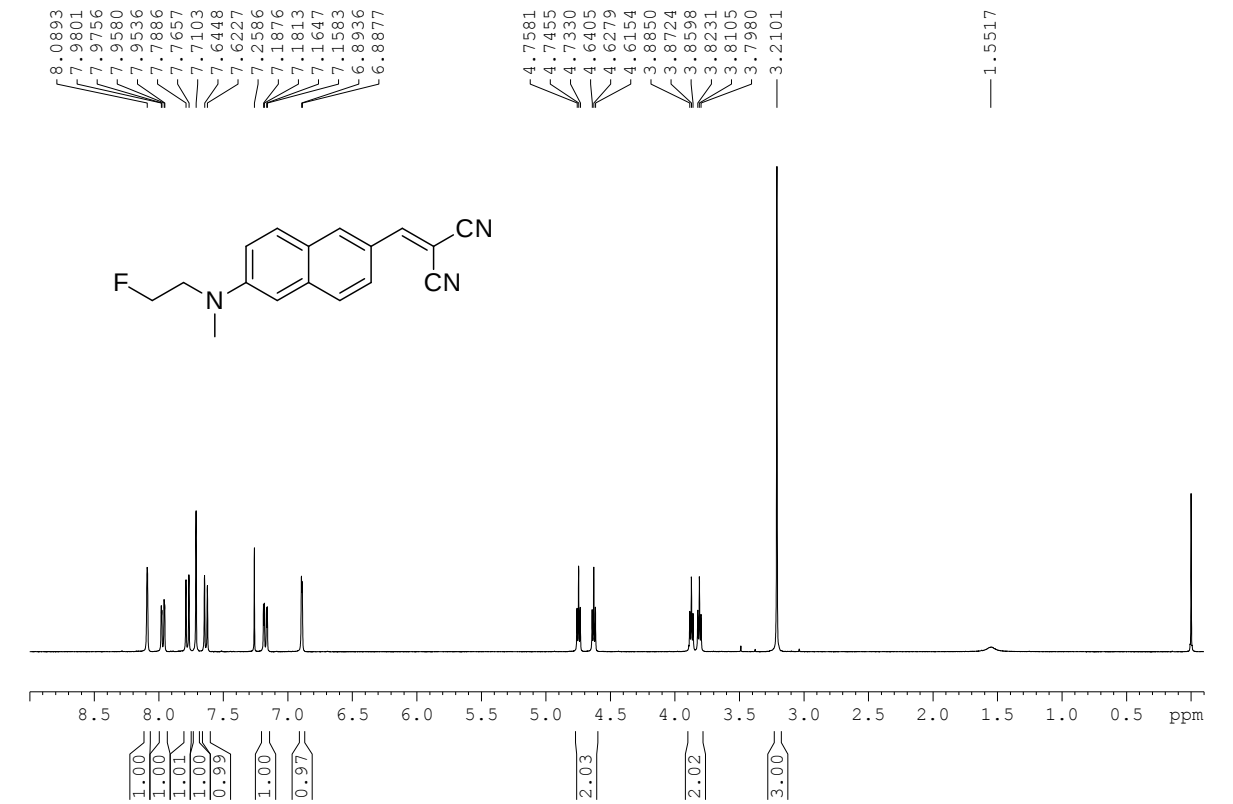
8.0893
7.9801
7.9756
7.9580
7.9536
7.7886
7.7657
7.7103
7.6448
7.6227
7.2586
7.1876
7.1813
7.1647
7.1583
6.8936
6.8877
4.7581
4.7455
4.7330
4.6405
4.6279
4.6154
3.8850
3.8724
3.8598
3.8231
3.8105
3.7980
3.2101
1.5517
CN
CN
F
N
8.5 8.0 7.5 7.0 6.5 6.0 5.5 5.0 4.5 4.0 3.5 3.0 2.5 2.0 1.5 1.0 0.5 ppm
1.00
1.00
1.01
1.00
0.99
1.00
0.97
2.03
2.02
3.00

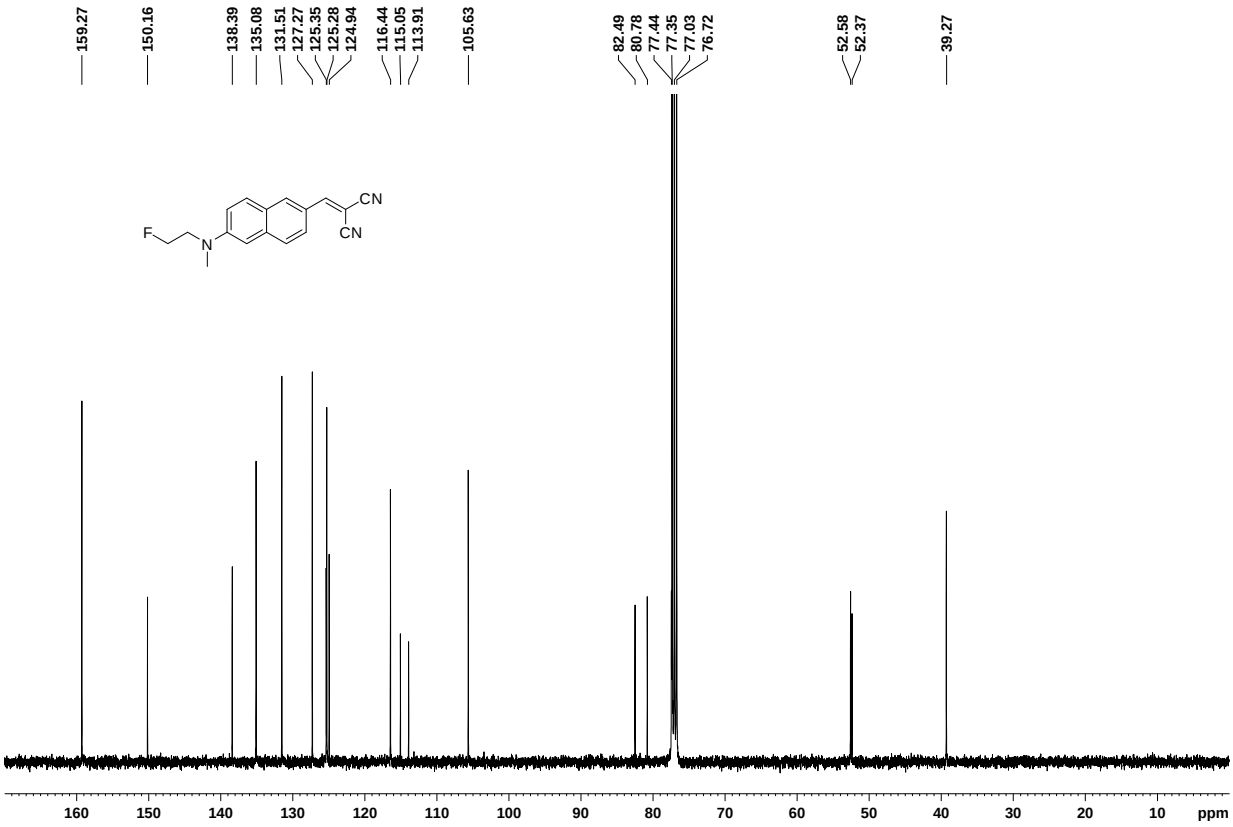
159.27
150.16
138.39
135.08
131.51
127.27
125.35
125.28
124.94
116.44
115.05
113.91
105.63
82.49
80.78
77.44
77.35
77.03
76.72
52.58
52.37
39.27
CN
CN
F
N
160 150 140 130 120 110 100 90 80 70 60 50 40 30 20 10 ppm

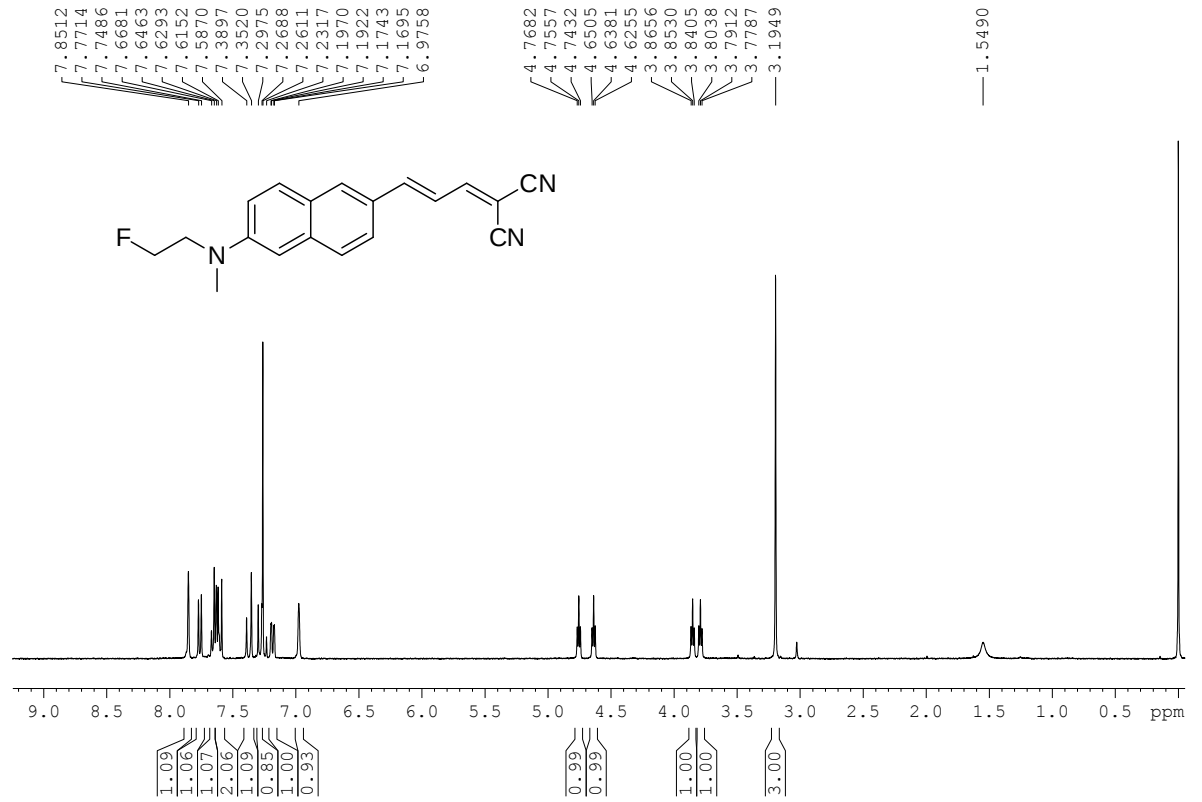
7.8512
7.7714
7.7486
7.6681
7.6463
7.6293
7.6152
7.5870
7.3897
7.3520
7.2975
7.2688
7.2611
7.2317
7.1970
7.1922
7.1743
7.1695
6.9758
4.7682
4.7557
4.7432
4.6505
4.6381
4.6255
3.8656
3.8530
3.8405
3.8038
3.7912
3.7787
3.1949
1.5490
CN
CN
F
N
9.0 8.5 8.0 7.5 7.0 6.5 6.0 5.5 5.0 4.5 4.0 3.5 3.0 2.5 2.0 1.5 1.0 0.5 ppm
1.09
1.06
1.07
2.06
1.09
0.85
1.00
0.93
0.99
0.99
1.00
1.00
3.00

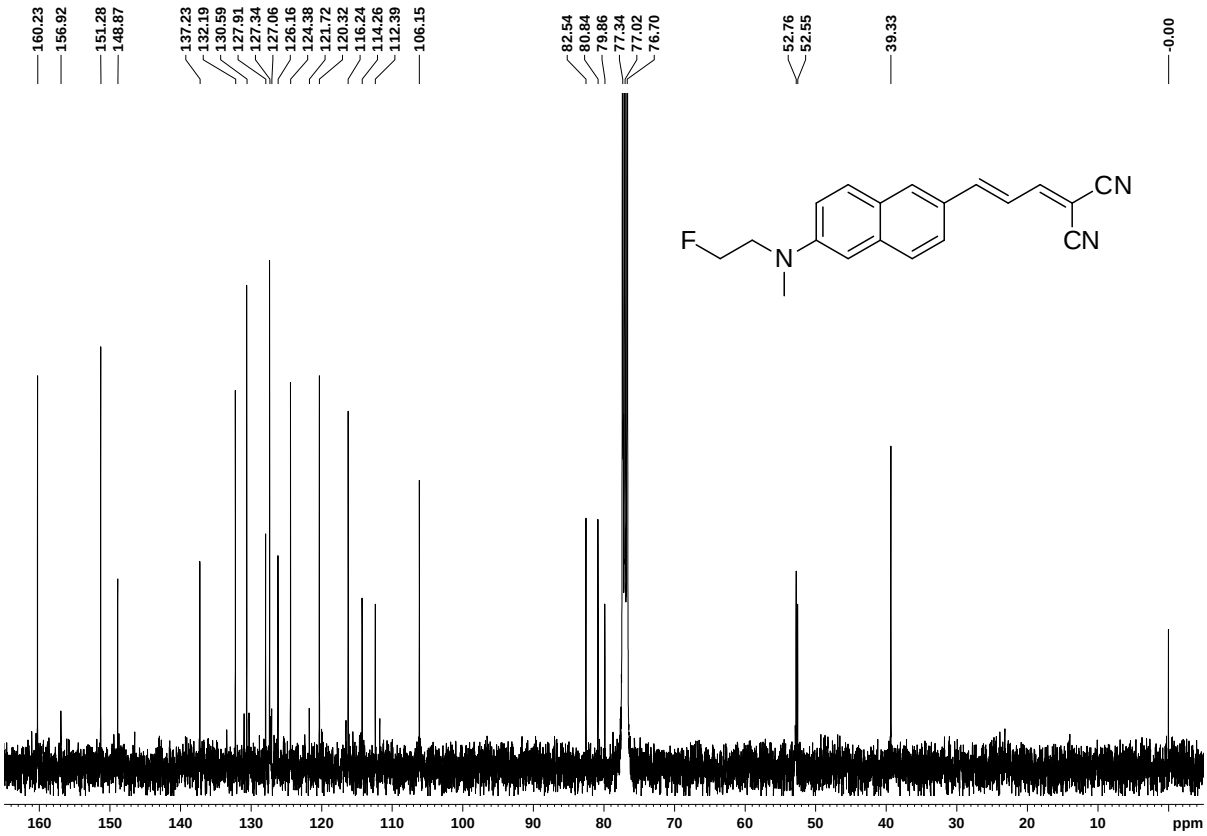
160.23
156.92
151.28
148.87
137.23
132.19
130.59
127.91
127.34
127.06
126.16
124.38
121.72
120.32
116.24
114.26
112.39
106.15
82.54
80.84
79.86
77.34
77.02
76.70
52.76
52.55
39.33
0.00
CN
CN
F
N
160 150 140 130 120 110 100 90 80 70 60 50 40 30 20 10 ppm

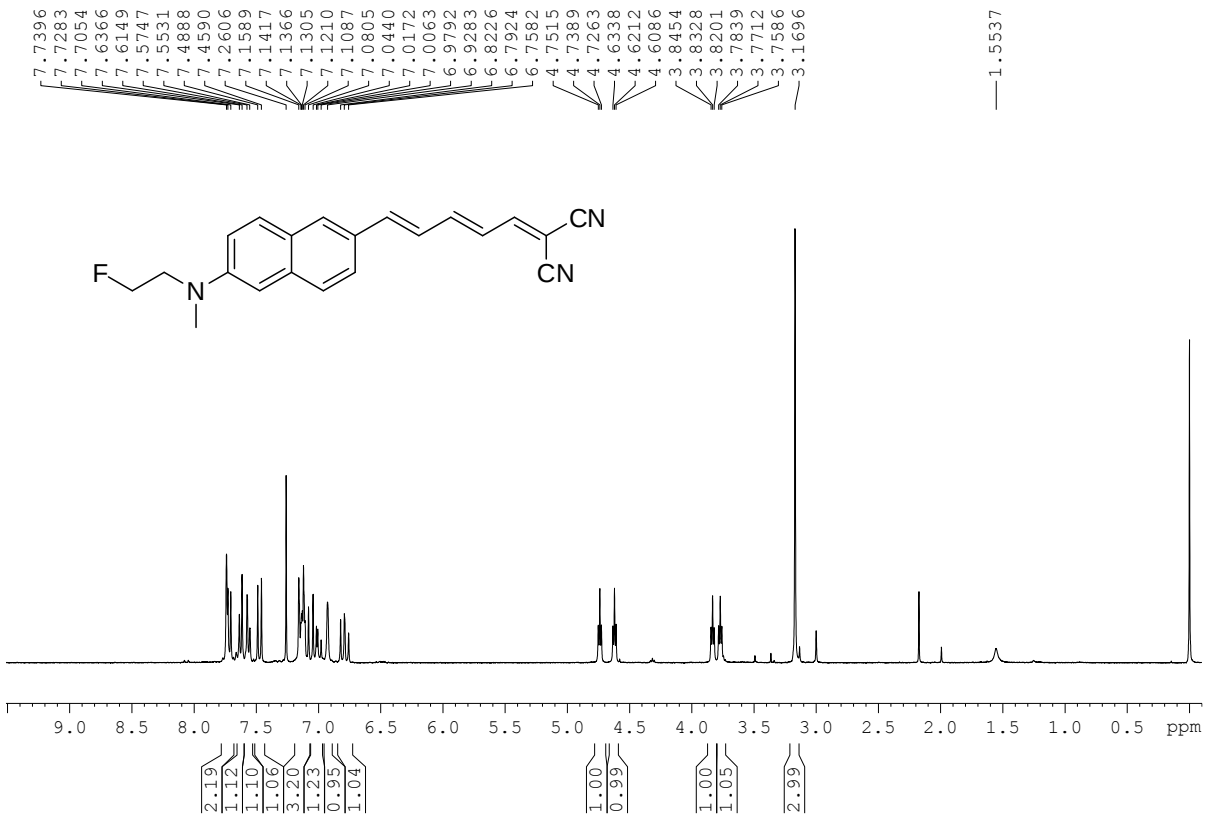
7.7396
7.7283
7.7054
7.6366
7.6149
7.5747
7.5531
7.4888
7.4590
7.2606
7.1589
7.1417
7.1366
7.1305
7.1210
7.1087
7.0805
7.0440
7.0172
7.0063
6.9792
6.9283
6.8226
6.7924
6.7582
4.7515
4.7389
4.7263
4.6338
4.6212
4.6086
3.8454
3.8328
3.8201
3.7839
3.7712
3.7586
3.1696
1.5537
F
N
CN
CN
9.0 8.5 8.0 7.5 7.0 6.5 6.0 5.5 5.0 4.5 4.0 3.5 3.0 2.5 2.0 1.5 1.0 0.5 ppm
2.19
1.12
1.10
1.06
3.20
1.23
0.95
1.04
1.00
0.99
1.00
1.05
2.99

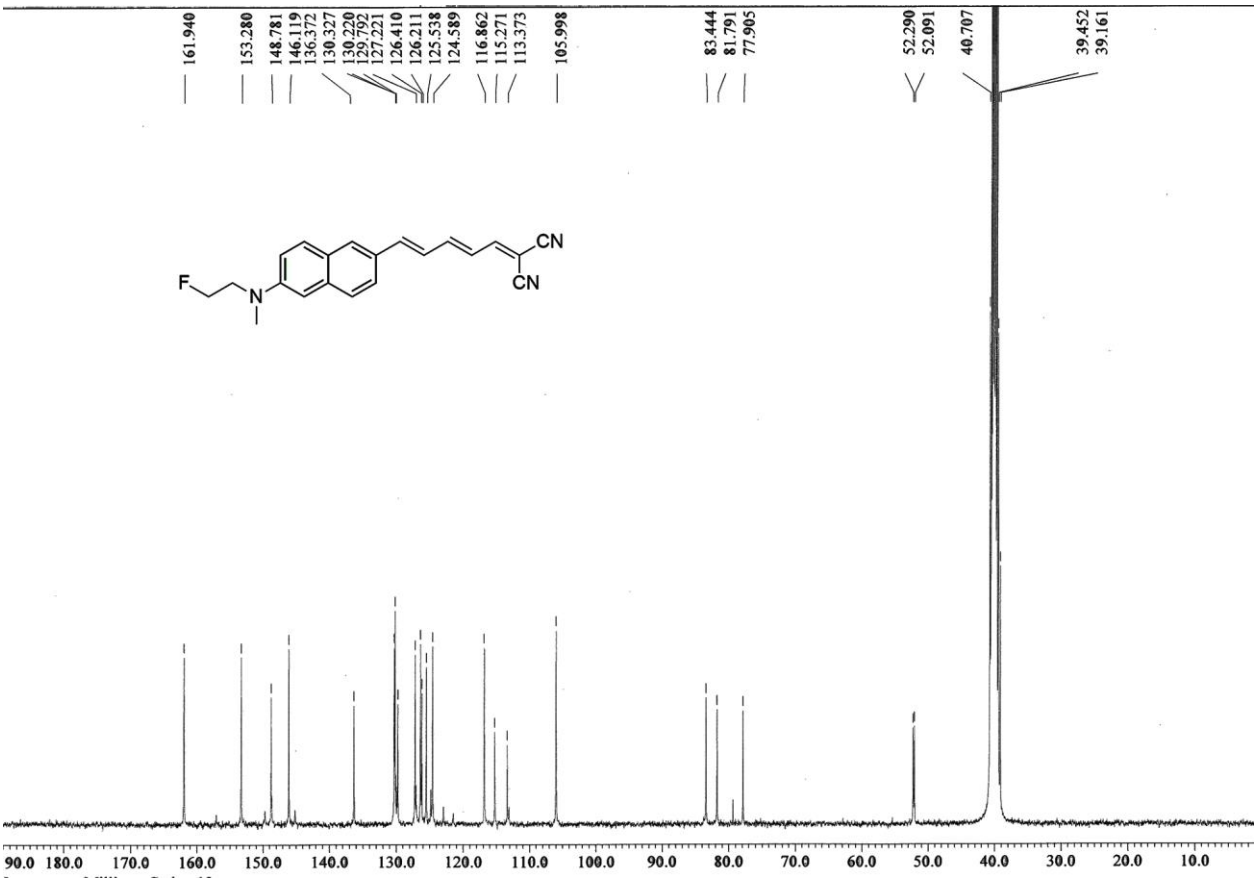
161.940
153.280
148.781
146.119
136.372
130.327
130.220
129.792
127.221
126.410
126.211
125.538
124.589
116.862
115.271
113.373
105.998
83.444
81.791
77.905
52.290
52.091
40.707
39.452
39.161
F
N
CN
CN
90.0 180.0 170.0 160.0 150.0 140.0 130.0 120.0 110.0 100.0 90.0 80.0 70.0 60.0 50.0 40.0 30.0 20.0 10.0

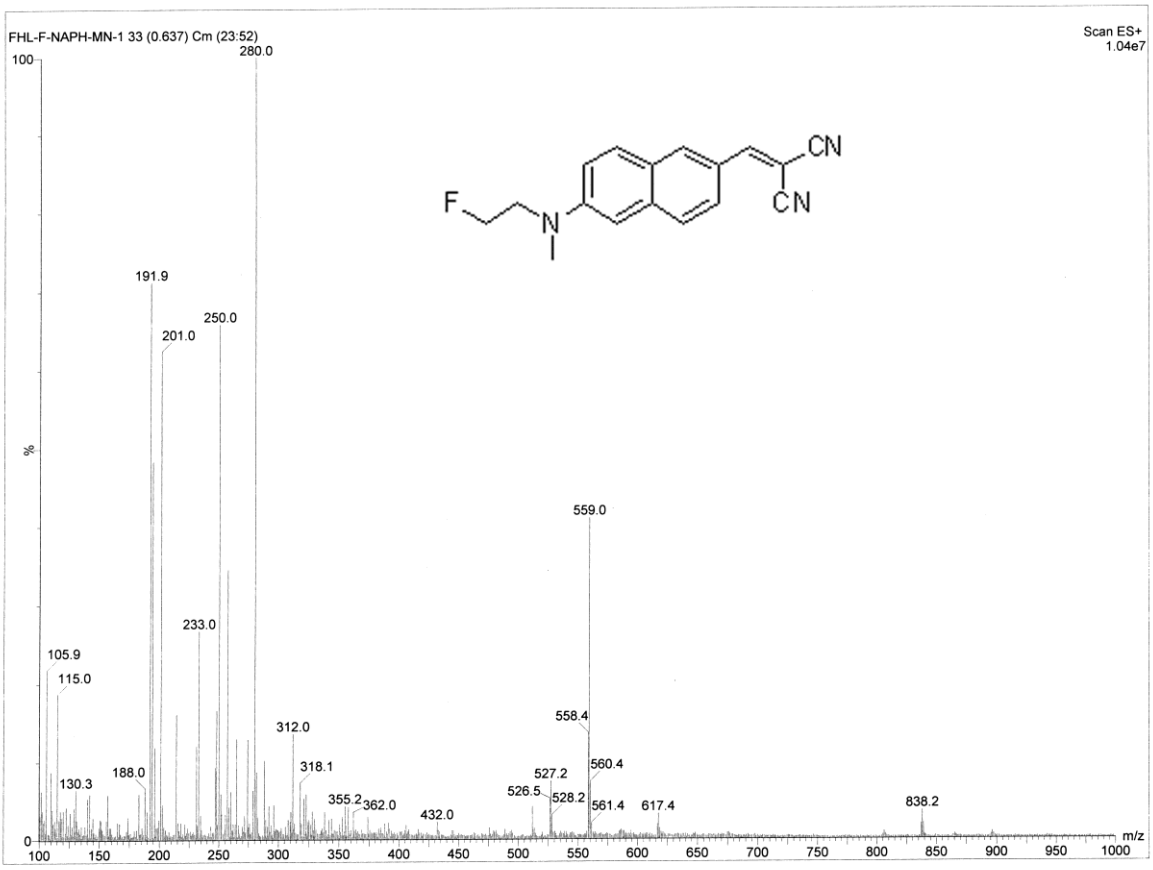

Elemental Composition Report

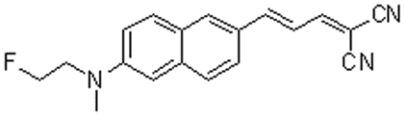

Single Mass Analysis
Tolerance = 5.0 PPM / DBE: min = -1.5, max = 100.0
Element prediction: Off
Number of isotope peaks used for i-FIT = 2

Monoisotopic Mass, Even Electron Ions
1794 formula(e) evaluated with 9 results within limits (up to 100 closest results for each mass)
Elements Used:
C: 0-50 H: 0-60 N: 0-15 O: 0-15 F: 0-3

FHL-NPF-2 8 (0.137)
TOF MS ES+
1.37e+004

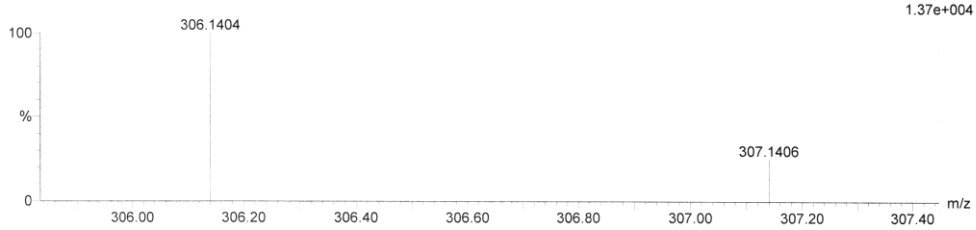

Mass	Calc. Mass	mDa	PPM	DBE	i-FIT	Formula
Minimum:				-1.5		
Maximum:		5.0	5.0	100.0		
306.1404	306.1403	0.1	0.3	5.5	334.6	C9 H15 N9 F3
	306.1407	-0.3	-1.0	12.5	15.2	C19 H17 N3 F
	306.1400	0.4	1.3	-1.5	502.5	C9 H24 N O10
	306.1400	0.4	1.3	9.5	338.5	C7 H12 N15
	306.1398	0.6	2.0	0.5	787.6	C3 H17 N11 O5 F
	306.1412	-0.8	-2.6	5.5	575.6	C4 H13 N15 O F
	306.1414	-1.0	-3.3	3.5	339.1	C10 H20 N5 O6
	306.1418	-1.4	-4.6	8.5	82.3	C16 H18 N3 O F2
	306.1389	1.5	4.9	0.5	498.6	C8 H19 N5 O4 F3

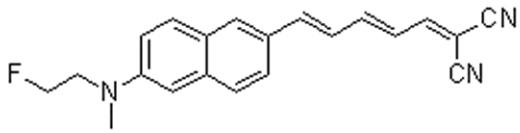

Elemental Composition Report

Single Mass Analysis
Tolerance = 5.0 PPM / DBE: min = -1.5, max = 100.0
Element prediction: Off
Number of isotope peaks used for i-FIT = 2

Monoisotopic Mass, Even Electron Ions
2159 formula(e) evaluated with 9 results within limits (up to 100 closest results for each mass)
Elements Used:
C: 0-50 H: 0-60 N: 0-15 O: 0-15 F: 0-3
FHL-NPF-3 1 (0.017)
TOF MS ES+

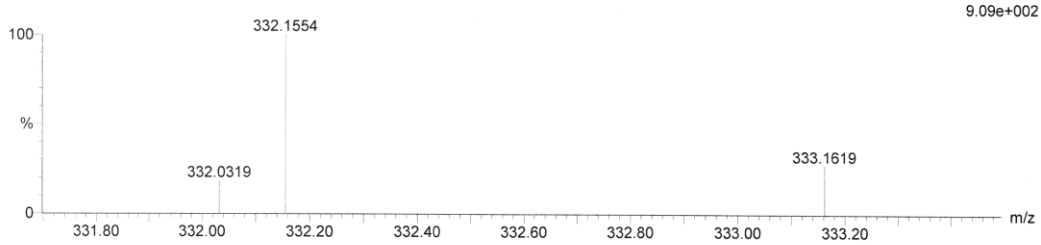

Minimum:				-1.5		
Maximum:		5.0	5.0	100.0		
Mass	Calc. Mass	mDa	PPM	DBE	i-FIT	Formula
332.1554	332.1555	-0.1	-0.3	1.5	47.3	C5 H19 N11 O5 F
	332.1557	-0.3	-0.9	-0.5	30.0	C11 H26 N O10
	332.1557	-0.3	-0.9	10.5	20.2	C9 H14 N15
	332.1559	-0.5	-1.5	6.5	19.9	C11 H17 N9 F3
	332.1546	0.8	2.4	1.5	29.8	C10 H21 N5 O4 F3
	332.1563	-0.9	-2.7	13.5	0.9	C21 H19 N3 F
	332.1543	1.1	3.3	5.5	30.2	C8 H18 N11 O4
	332.1568	-1.4	-4.2	6.5	34.5	C6 H15 N15 O F
	332.1570	-1.6	-4.8	4.5	20.1	C12 H22 N5 O6

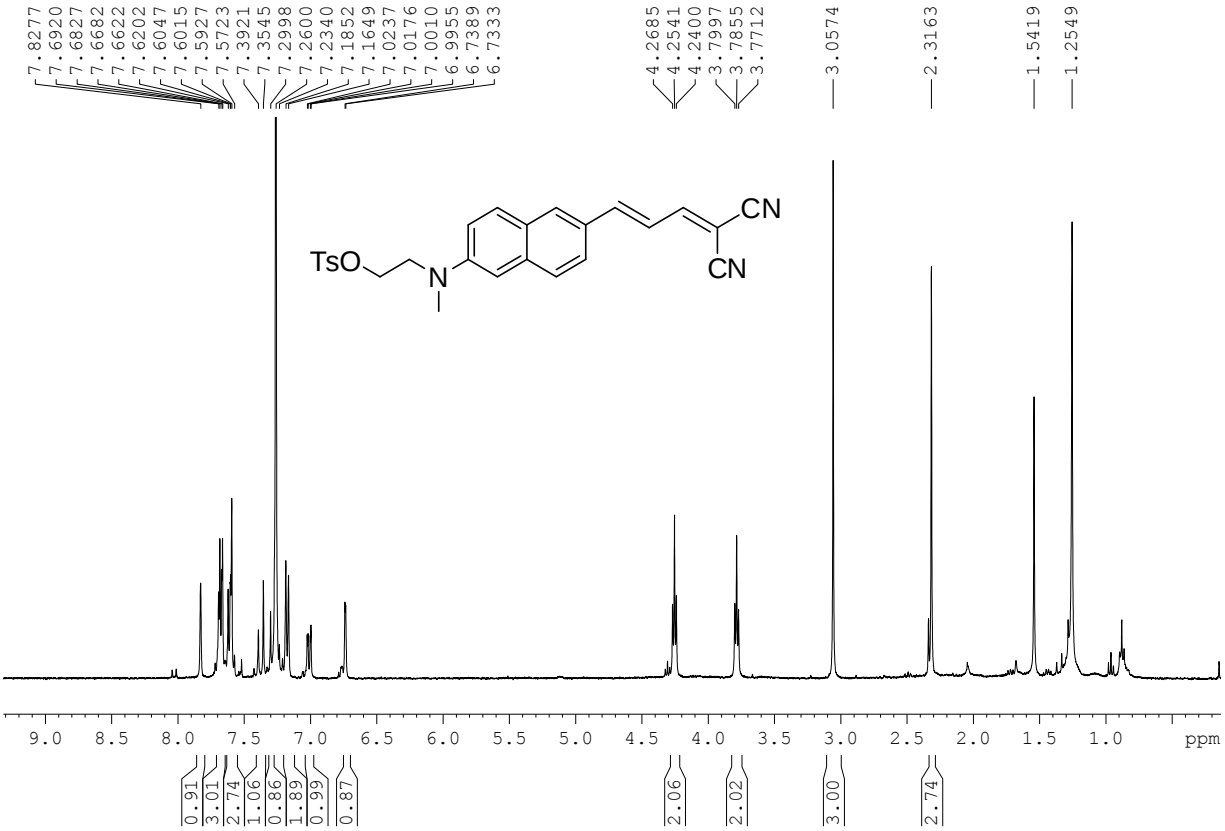

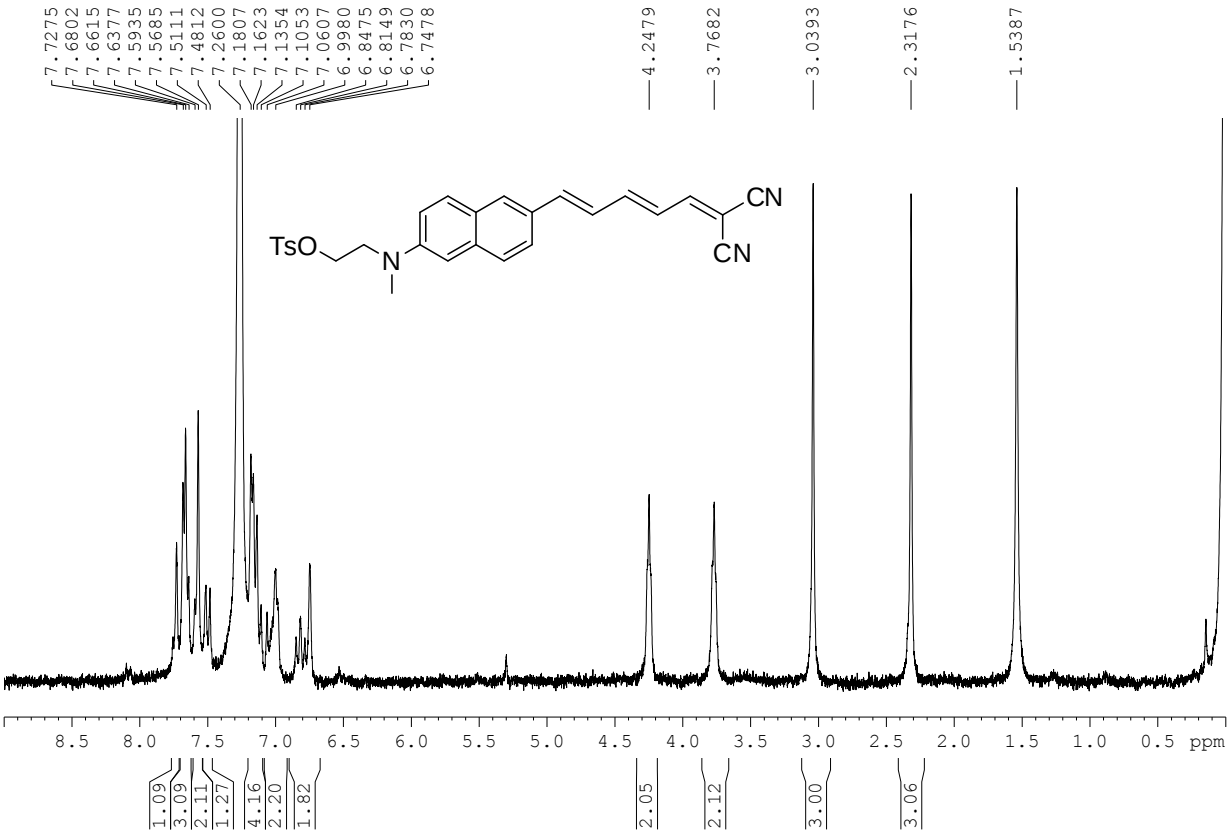

References

1. Z. Li, M. Cui, J. Dai, X. Wang, P. Yu, Y. Yang, J. Jia, H. Fu, M. Ono, H. Jia, H. Saji and B. Liu, *J. Med. Chem.*, 2013, **56**, 471-482.
2. H. Fu, P. Tu, L. Zhao, J. Dai, B. Liu and M. Cui, *Anal. Chem.*, 2016, **88**, 1944-1950.
3. H. L. Fu, M. C. Cui, L. Zhao, P. Y. Tu, K. X. Zhou, J. P. Dai and B. L. Liu, *J. Med. Chem.*, 2015, **58**, 6972-6983.
4. M. Cui, X. Wang, P. Yu, J. Zhang, Z. Li, X. Zhang, Y. Yang, M. Ono, H. Jia, H. Saji and B. Liu, *J. Med. Chem.*, 2012, **55**, 9283-9296.
5. Y. Yang, M. Cui, X. Zhang, J. Dai, Z. Zhang, C. Lin, Y. Guo and B. Liu, *J. Med. Chem.*, 2014, **57**, 6030-6042.
6. H. Fu, M. Cui, P. Tu, Z. Pan and B. Liu, *Chem. Commun. (Camb)*, 2014, **50**, 11875-11878.